ACS Partner Journal

CHEM & BIO ENGINEERING

pubs.acs.org/ChemBioEng

Review

Manganese-Based Oxide Cathode Materials for Aqueous Zinc-Ion Batteries: Materials, Mechanism, Challenges, and Strategies

Published as part of Chem & Bio Engineering virtual special issue "Secondary Batteries".

Bao Zhang, Peng Dong, Shouyi Yuan,* Yannan Zhang,* Yingjie Zhang, and Yonggang Wang*

Cite This: *Chem Bio Eng.* 2024, 1, 113−132

Read Online

ABSTRACT: Aqueous zinc-ion batteries (AZIBs) have recently attracted worldwide attention due to the natural abundance of Zn, low cost, high safety, and environmental benignity. Up to the present, several kinds of cathode materials have been employed for aqueous zinc-ion batteries, including manganese-based, vanadium-based, organic electrode materials, Prussian Blues, and their analogues, etc. Among all the cathode materials, manganese (Mn)-based oxide cathode materials possess the advantages of low cost, high theoretical specific capacity, and abundance of reserves, making them the most promising cathode materials for commercialization. However, several critical issues, including intrinsically poor conductivity, sluggish diffusion kinetics of Zn^{2+}, Jahn−Teller effect, and Mn dissolution, hinder their practical applications. This Review provides an overview of the development history, research status, and scientific challenges of manganese-based oxide cathode materials for aqueous zinc-ion batteries. In addition, the failure mechanisms of manganese-based oxide materials are also discussed. To address the issues facing manganese-based oxide cathode materials, various strategies, including pre-intercalation, defect engineering, interface modification, morphology regulation, electrolyte optimization, composite construction, and activation of dissolution/deposition mechanism, are summarized. Finally, based on the analysis above, we provide future guidelines for designing Mn-based oxide cathode materials for aqueous zinc-ion batteries.

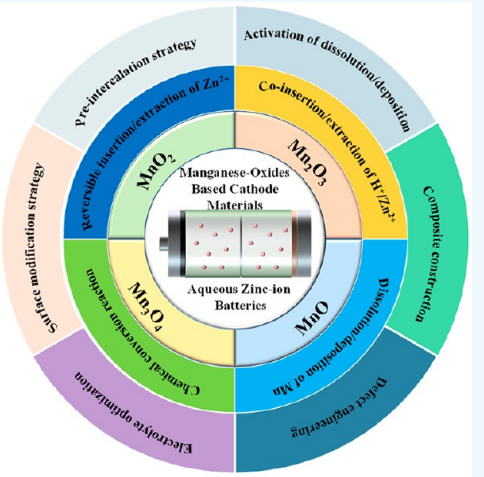

KEYWORDS: *aqueous zinc-ion batteries, manganese-based oxide materials, cathode, energy storage mechanism, failure mechanisms, modification strategies*

1. INTRODUCTION

With the gradual exhaustion of non-renewable resources such as fossil fuels, the development of sustainable renewable energy has become the theme of the current period.[1−3] Although conventional renewable energies such as wind, solar, and tidal energies are naturally abundant, intermittent access and poor stability limit their application in the field of large-scale energy storage and conversion.[4−6] Under such circumstances, chemical power sources have emerged as complementary sources for energy storage and conversion.[7] At present, several kinds of secondary batteries, including lead-acid batteries, alkaline nickel/cadmium batteries, and lithium-ion batteries, have been commercialized for electrochemical energy storage.[8,9] However, lead-acid batteries and alkaline nickel/cadmium batteries exhibit relatively low energy density and are harmful to human health due to the use of toxic metals in the batteries.[10,11] Since their commercialization, lithium-ion batteries (LIBs) have dominated the market of energy storage systems (ESS) due to their light weight, high energy density, and high specific power.[12−14] Unfortunately, the use of expensive metals such as Li, Co, and Ni leads to an increase in manufacturing costs.[15,16] Meanwhile, the organic electrolytes inside the LIBs are highly flammable, which brings about a serious safety hazard in practical applications.[17,18]

Compared with conventional LIBs, aqueous batteries are promising for large-scale electrochemical energy storage owing to low cost, environmental benignity, and high operational safety.[19,20] Moreover, the aqueous electrolyte can effectively prevent safety issues such as fire and explosion.[21−23] In recent years, aqueous multivalent ion batteries, especially aqueous zinc-ion batteries, aqueous aluminum-ion batteries, aqueous calcium-ion batteries, etc., have attracted much attention from

Received: December 21, 2023
Accepted: February 7, 2024
Published: March 7, 2024

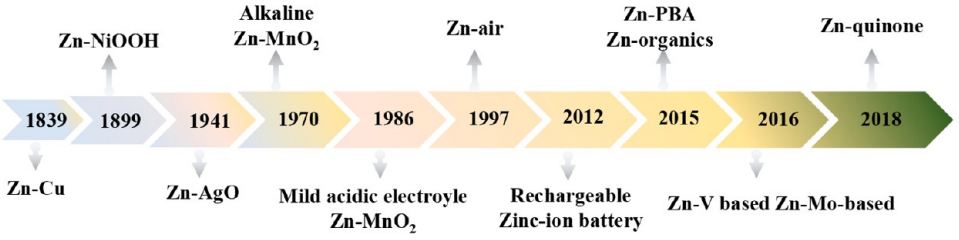

Figure 1. History of the development of zinc-ion batteries.

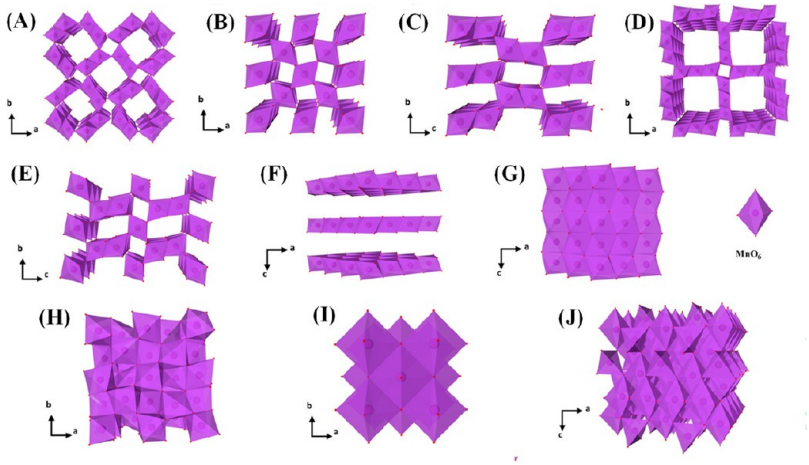

Figure 2. Crystal structures of (A) α-MnO_2, (B) β-MnO_2, (C) R-MnO_2, (D) T-MnO_2, (E) γ-MnO_2, (F) δ-MnO_2, (G) ε-MnO_2, (H) Mn_2O_3, (I) MnO, and (J) Mn_3O_4 are displayed. Reproduced with permission from ref 27. Copyright 2022, The Authors.

researchers owing to their high energy density.[24] Typically, the volumetric energy density of multivalent-ion batteries are much higher than that of monovalent-ion batteries because multivalent ions can transfer multiple electrons per ion. Hence, when the same redox active sites are provided, multivalent-ion batteries will obtain a higher capacity than that of monovalent-ion batteries.[25,26]

Aqueous zinc-ion batteries have gained a lot of attention from researchers owing to high capacity, abundance of reserves, low cost, high safety, and environmental benignity.[27] In fact, the development of aqueous zinc-ion batteries has a long history. As early as 1800, Alessandro Volta invented the first Zn-based "voltaic cell" by separating the Zn anode and Cu cathode with cardboard or cloth soaked in saline water. Subsequently, Leclanche proposed the prototype Zn−Mn battery, which employed metallic Zn as the anode, MnO_2 as the cathode, and NH_4Cl aqueous solution as the electrolyte.[28] Thereafter, through years of exploration, a variety of Zn batteries, such as Zn−AgO-, Zn−NiOOH-, alkaline Zn−MnO_2-, Zn−air-, Zn−V-, and Zn−Mo-based batteries, have been proposed.[29] Yet, the severe corrosion of Zn metal in the alkaline electrolyte during cycles gives rise to the rapidly deteriorative cycling performance of Zn metal batteries.[30] In 1986, Yamamoto *et al.* successfully developed the aqueous Zn/$ZnSO_4$/MnO_2 battery by replacing the alkaline electrolyte of the alkaline Zn/Mn battery with a $ZnSO_4$ aqueous solution. They proved that the introduction of a slightly acidic electrolyte could markedly weaken the passivation effect of Zn metal, greatly improving the anode reversibility and thereby enabling the enhanced cycling stability of the battery.[31] Until 2011, Kang *et al.* put forward a $ZnSO_4$ electrolyte-based Zn/Mn battery, revealing that the migration of Zn^{2+} ions endowed the MnO_2 cathode with charge-storage property. Besides, they pointed out that MnO_2 with other structures also shows the identical energy-storage behavior.[32] Since then, many efforts have been devoted to investigating various AZIBs operating in neutral or weakly acidic aqueous electrolytes (Figure 1).[33] Typically, several kinds of intercalation cathodes have previously employed for AZIBs including Mn-based,[34−36] V-based,[37−40] Prussian blue analogues,[41−43] organic compounds,[44−46] *etc.* Among them, Mn-based oxide cathode materials are considered to be one of the most promising materials, owing to their high capacity, high operating voltage, low cost, and nontoxicity.[47]

In this Review, the characteristics, existing problems, and current research progress of Mn-based oxide cathode materials are comprehensively summarized, and the energy storage mechanism for Mn-based aqueous zinc-ion battery is deeply clarified. Additionally, various modification strategies from the following aspects of pre-intercalation, defect engineering, interface modification, electrolyte optimization, and morphology regulation are proposed.

2. CRYSTAL STRUCTURE OF MN-OXIDE-BASED CATHODE MATERIALS

The Mn-based materials exhibit the advantages of a high theoretical specific capacity of 308 mAh g^{-1} (Mn^{4+}/Mn^{3+}) and stable operating voltage (~1.4 V), as well as large reserves, low cost, and nontoxicity, which are extensively applied in the field of energy storage.[48] Various valence states of the Mn element, such as Mn^{2+}, Mn^{3+}, Mn^{4+}, Mn^{7+}, *etc.*, enable abundant structures of Mn-based compounds.[49] Figure 2 displays the crystal structures of MnO_2, Mn_2O_3, Mn_3O_4, and MnO.[50] As shown in Figure 2A−H, both MnO_2 and Mn_2O_3 are generally formed by connecting edge-sharing or corner-sharing [MnO_6]

https://doi.org/10.1021/cbe.3c00120
Chem Bio Eng. 2024, 1, 113−132

octahedra as the basic structural unit.[51] Meanwhile, MnO exhibits a typical NaCl-type face-centered cubic crystal structure, and Mn_3O_4 is the mixture of Mn_2O_3 and MnO, as shown in Figure 2I,J.[52] The detailed structures of these Mn-oxide-based materials are further discussed below.

2.1. MnO_2. The MnO_2 is formed by connecting edge-sharing or corner-sharing [MnO_6] octahedra as the basic structural unit. Different connecting modes contribute to various crystal structures of MnO_2.[53] Based on the connecting types between [MnO_6] octahedra, MnO_2 can be classified into the following structures: (1) tunnel-type structures, *e.g.*, α-MnO_2 (2×2 (4.6×4.6 Å^2)), β-MnO_2 (1×1 (2.3×2.3 Å^2)), R-MnO_2 (1×2), γ-MnO_2 (1×1 and 1×2 (2.3×4.6 Å^2)), T-MnO_2 (3×3 (7×7 Å^2));[54−56] (2) layered structures, *e.g.*, δ-MnO_2;[57,58] and (3) three-dimensional structures (3D), *e.g.*, λ-MnO_2 and ε-MnO_2 (Figure 3). All of the above MnO_2 with different crystal structures can serve as hosts for reversible Zn^{2+} storage. Nevertheless, the ion diffusion pathways differ in different crystal structures of Mn-based oxide, thus presenting varying energy storage capabilities and even energy storage mechanisms.[59]

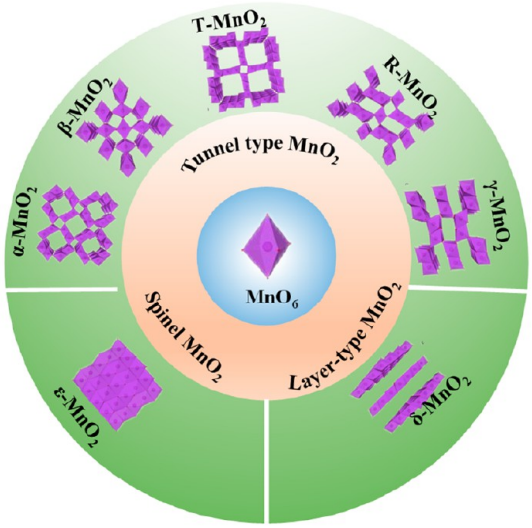

Figure 3. Crystal structures of (A) α-MnO_2, (B) β-MnO_2, (C) R-MnO_2, (D) T-MnO_2, (E) γ-MnO_2, and (F) δ-MnO_2. Adapted with permission from ref 27. Copyright 2022, The Authors.

As shown in Figure 3, the tunnel structure can accommodate the reversible insertion/extraction of Zn^{2+} in the tunnel space. The tunnel-type MnO_2 has a variety of crystal structures with different tunnel sizes, including α-MnO_2 (2×2 (4.6×4.6 Å^2)), β-MnO_2 (1×1 (2.3×2.3 Å^2)), γ-MnO_2 (1×1 and 1×2 (2.3×4.6 Å^2)), T-MnO_2 (3×3 (7×7 Å^2), *etc.*[60] Among them, α-MnO_2 with a 2×2 tunnel structure is considered an ideal cathode material for aqueous zinc-ion batteries. The large tunnel structure facilitates the rapid ion migration in the tunnel space. However, the reaction process is complicated, involving the transformation from the tunnel structure into the layered Zn buserite structure during the insertion of Zn^{2+}. Additionally, Mn^{4+} is reduced to Mn^{3+} during discharging. The disproportionation reaction of Mn^{3+} generates soluble Mn^{2+}, thus resulting in the loss of active materials and consequently rapid decay of capacity.[61]

The β-MnO_2 with a 1×1 tunnel structure is regarded as the most stable tunnel-type MnO_2. However, its narrow crystal structure limits the insertion/extraction of Zn^{2+}, leading to poor electrochemical performance. Besides, a similar transformation into the layered Zn buserite structure is also detected for β-MnO_2 during cycling, which may be beneficial for the insertion/extraction of Zn^{2+}.[62]

The γ-MnO_2 is made up of randomly arranged 1×1 and 1×2 tunnel structures. The structure is also not suitable for the insertion of Zn^{2+} ions. Specifically, at the beginning of Zn^{2+} insertion, the tunnel structure is partially transformed into spinel $ZnMn_2O_4$, followed by the formation of tunnel-type γ-Zn_xMnO_2. Later, part of γ-Zn_xMnO_2 is further converted to L-Zn_xMnO_2 with the continuous insertion of Zn^{2+}. Finally, after the complete insertion of Zn^{2+}, the crystal turns into a three-phase mixture consisting of $ZnMn_2O_4$, γ-Zn_xMnO_2, and L-Zn_xMnO_2. This complicated phase transition process is harmful to the insertion/extraction of Zn^{2+}.[63]

The T-MnO_2 exhibits a 3×3 (7.0×7.0 Å^2) tunnel structure, which contributes to the excellent ion transport and storage in the tunnel structure. However, to maintain structural stability, a lot of impurity cations and water molecules generally exist in the tunnel channels of T-MnO_2, which conversely restrict the diffusion and storage of ions in crystals. Moreover, the complicated preparation process of T-MnO_2 also limits its application.[52]

The δ-MnO_2 has a layered structure with a layer spacing of ~0.7 nm, which is larger than the radius of other tunnel-type MnO_2. Such a wide layer space provides more active sites for the rapid transport of Zn^{2+}. However, the layered structure will collapse under long-term cycles, resulting in the irreversible phase transition during cycling. This process is accompanied by a significant volume change, structural collapse, and Mn dissolution, consequently leading to the degeneration of rate and cycling performance.[64]

The λ-MnO_2 is a three-dimensional spinel-type structure, where O and Mn ions occupy the octahedral 32e and 16d positions, respectively. In regard to 3D λ-MnO_2, the insertion of cations into close-packed structures without tunnels or interlayer spaces is difficult, inducing a low initial capacity. Hence, spinel MnO_2 is considered unfavorable for the diffusion and storage of Zn^{2+}. For example, Cao *et al.* designed a porous λ-MnO_2 with open channels by treating spinel $LiMn_2O_4$ with acid. Such proposed λ-MnO_2 delivers a discharge capacity of 152 mAh g^{-1} under a current density of 68 mA g^{-1} in $ZnSO_4$ electrolyte.[65]

The ε-MnO_2 is formed by the dense packing of [MnO_6] octahedra. This structure is unfavorable for the de/intercalation of ions and protons during energy storage, and its intrinsic low electrochemical activity and low conductivity result in poor electrochemical performance.[66] The electrochemical performance of ε-MnO_2 can be improved by adjusting the structure and introducing defects to increase active sites.[27] Zhang *et al.* introduced structural water, nitrogen, and oxygen vacancies into ε-MnO_2 through ball milling. The embedding of crystal water in (102) and (110) crystal planes reduces the electrostatic interaction between zinc ions and ε-MnO_2, effectively promoting ion diffusion. Doping nitrogen significantly enhances the storage capacity of oxygen vacancies for H^+ ions, thereby improving the capacity of ε-MnO_2.[67]

2.2. Mn_2O_3. The Mn_2O_3 belongs to the orthorhombic system with MnO as the basic unit. The Mn^{3+} exhibits an octahedral coordination, while the O^{2-} shows a tetrahedral coordination. Unlike MnO_2 composites with tunable Zn

https://doi.org/10.1021/cbe.3c00120
Chem Bio Eng. 2024, 1, 113−132

insertion pathways, the migration path of Zn^{2+} is blocked, resulting in limited initial specific capacity and cycling stability. During cycles, the Mn_2O_3 composites suffer from a phase transition from the orthorhombic structure to the layered structure with the continuous insertion of Zn^{2+}, leading to Mn^{2+} dissolution.[68] For example, Kang's group revealed that α-Mn_2O_3 could be converted into layered Zn-birnessite during cycling, thereby realizing the reversible insertion/extraction of Zn^{2+}.[69]

2.3. Mn_3O_4. The Mn_3O_4 possesses two oxidation states, Mn^{2+} and Mn^{3+}. Mn^{2+} and Mn^{3+} ions occupy the tetrahedral (4a) and octahedral (8d) positions, respectively, in a distorted cubic close-packed array of oxygen atoms. Mn_3O_4 has a theoretical specific capacity of 468.5 mAh g^{-1}. Similar to other manganese-based oxides, Mn_3O_4 experiences capacity decay and poor rate performance due to its poor conductivity and the dissolution of Mn^{2+}.[70] In addition, the strong electrostatic interaction between the spinel Mn_3O_4 crystal skeleton and Zn^{2+} also leads to the degradation of electrochemical performance.

2.4. MnO. Manganese oxide (MnO) exhibits a typical face-centered cubic (*fcc*) structure with a high theoretical specific capacity (755 mAh g^{-1}). However, practical applications of MnO are hindered by a series of issues, including the lack of tunnel structures, low electronic conductivity, severe structural collapse, poor rate performance, and cycling stability. It is worth noting that Mn defects can be formed during the initial charging of MnO, thus activating the electrochemical performance of MnO. The formation of Mn defects provides a narrow energy barrier for Zn^{2+} migration, promoting the reversible insertion/extraction of Zn^{2+} in MnO host. Therefore, by introducing manganese defects or oxygen vacancies, constructing protective layers, regulating morphology, and preparing heterostructures, the above-mentioned issues can be effectively overcome, improving the electrochemical performance of MnO.[71,72] Electrochemical performance of various Mn-based cathode materials for AZIBs are shown in Tables 1.

Table 1. Electrochemical Performance of Various Mn-Based Cathode Materials for AZIBs

Cathode	Electrolyte	Voltage (V)	Specific capacity (mAh g^{-1})	Ref
K^+-intercalated δ-MnO_2	2 M $ZnSO_4$ + 0.5 M $MnSO_4$	0.8−1.8	419 at 0.5 A g^{-1}	73
Al-doped MnO_2	2 M $ZnSO_4$ + 0.1 M $MnSO_4$	0.8−1.8	327.9 at 0.2 A g^{-1}	74
Cu-δ-MnO_2	2 M $ZnSO_4$ + 0.3 M $MnSO_4$	0.9−1.9	153 at 3 A g^{-1}	75
MnO_2/Graphite Nanocomposite	3 M $ZnSO_4$ + 0.1 M $MnSO_4$	0.8−1.8	310 at 0.1 A g^{-1}	67
α-MnO_2/MGS	2 M $ZnSO_4$ + 0.2 M $MnSO_4$	1.0−1.85	382.2 at 0.3 A g^{-1}	76
α-MnO_2	1 M $ZnSO_4$	1.0−1.8	233 at 83 mA g^{-1}	54
β-MnO_2	1 M $ZnSO_4$	1.0−1.8	270 at 0.1 A g^{-1}	56
Eu doping β-MnO_2	2 M $ZnSO_4$ + 0.1 M $MnSO_4$	0.8−1.9	409 at 0.2 A g^{-1}	77
MnO_2@AEPA	2 M $ZnSO_4$ + 0.1 M $MnSO_4$	0.8−1.9	223 at 0.5 A g^{-1}	78
γ-MnO_2	1 M $Zn(CH_3COO)_2$ + 0.4 M $Mn(CH_3COO)_2$	1.0−1.8	556 at 5 mA cm^{-2}	79
δ-MnO_2	2 M $ZnSO_4$ + 0.1 M $MnSO_4$	1.0−1.8	636 at 0.1 A g^{-1}	80
δ-MnO_2	2 M $ZnSO_4$ + 0.2 M $MnSO_4$	0.9−1.9	278 at 1 C	81
ε-MnO_2@N	2 M $ZnSO_4$ + 0.5 M $MnSO_4$	1.0−1.8	124 at 5.0 A g^{-1}	66
T-MnO_2	1 M $ZnSO_4$	0.7−1.9	150 at C/20	82
MnO	2 M $ZnSO_4$ + 0.1 M $MnSO_4$	0.8−1.8	283.1 at 0.1 A g^{-1}	83
MnO	2 M $ZnSO_4$ + 0.1 M $MnSO_4$	1.0−1.9	330 at 0.1 A g^{-1}	84
MnO_x	1 M $ZnSO_4$ + 0.3 M $MnSO_4$	0.8−1.8	845 at 0.1 A g^{-1}	85
MnO_x@N−C	2 M $ZnSO_4$ + 0.1 M $MnSO_4$	0.8−1.8	305 at 0.5 A g^{-1}	86
α-Mn_2O_3	2 M $ZnSO_4$	1.0−1.9	148 at 100 mA g^{-1}	69
Mn_3O_4	1 M $ZnSO_4$ + 1 M $MnSO_4$	0.6−1.9	221 at 100 mA g^{-1}	87
Mn_3O_4	2 M $ZnSO_4$	0.8−1.9	239.2 at 0.1 A g^{-1}	88
Mn_3O_4	2 M $ZnSO_4$ + 0.24 M $MnSO_4$	0.2−1.85	396.2 at 0.2 A g^{-1}	89

3. ENERGY STORAGE MECHANISM OF ZN/MNO_X BATTERIES

Due to the multiple oxidation states of Mn, the unstable structure of MnOx, as well as theside side reactions in aqueous solutions, the Zn/MnO_x batteries present a quite complicated mechanism of cathode reactions. Meanwhile, the energy storage of Zn/MnO_x batteries is also associated with the pH, additives, and salts of the electrolytes. Up to now, a variety of controversial energy-storage mechanisms have been proposed.[90,91] Overall, the energy-storage mechanisms can be divided into the following four categories: (1) insertion/extraction of Zn^{2+}, (2) chemical conversion reaction model, (3) co-insertion/extraction of H^+/Zn^{2+}, and (4) dissolution/deposition mechanism, as shown in Figure 4.[92]

3.1. Reversible Insertion/Extraction of Zn^{2+}. Due to the similar ionic radius of Zn^{2+} (0.74 Å) and Li^+ (0.76 Å), they share a similar energy storage mechanism. Therefore, Zn ions are able to reversibly insert and extract, as shown in Figure 5A.[69] However, compared with Li ions, Zn ions display a larger solvation sheath and electrostatic repulsion due to their higher charge. Moreover, the Zn ions can be solvated with H_2O to form hydrated Zn ions with a large molecular radius via hydrogen bonding, leading to sluggish solid-phase diffusion kinetics of Zn ions. In this case, to realize fast intercalation/de-intercalation kinetics in the host materials, a large layered space is required.[93] For example, in 2012, Kang *et al.* discovered the reversible migration of Zn ions between the Zn anode and α-MnO_2 cathode to achieve charge storage, as shown in Figure. 5C. They also found that the α-MnO_2 reversibly transformed into spinel $ZnMn_2O_4$ after Zn^{2+} intercalation, as follows:[32]

$$Zn^{2+} + 2e^- + 2MnO_2 \leftrightarrow ZnMn_2O_4$$

$$Zn \leftrightarrow Zn^{2+} + 2e^-$$

Alfaruqi *et al.* also showed that in the electrochemical zinc insertion process, the layered MnO_2 will undergo structural transformation into layered Zn_xMnO_2, and the process of zinc-ion insertion in layered MnO_2 is shown in Figure 5B.[94] They studied the structural transformation of γ-MnO_2 during the electrochemical reaction and showed that the structural transformation of tunneled γ-MnO_2 into the spinel-type phase of Mn(III) ($ZnMn_2O_4$) and the γ-Zn_xMnO_2 (tunnel-type) and L-Zn_yMnO_2 (layered-type) of two Mn(II). As illustrated in Figure 5D, Kim *et al.* analyzed the structural

https://doi.org/10.1021/cbe.3c00120
Chem Bio Eng. 2024, 1, 113−132

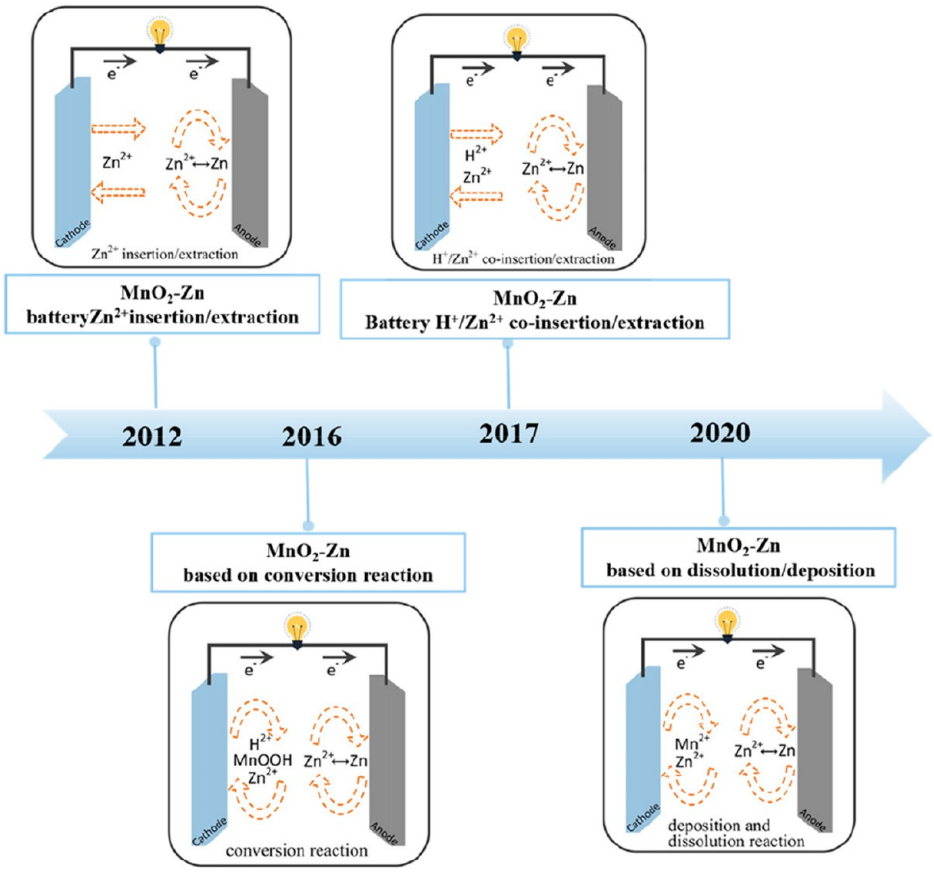

Figure 4. Development of AZIBs energy storage mechanism and schematic diagram of its mechanism. Reproduced with permission from ref 92. Copyright 2020, Science Press and Dalian Institute of Chemical Physics, Chinese Academy of Sciences.

evolution of layered manganese dioxide during the insertion of zinc ions using *in situ* synchrotron, *ex situ* X-ray diffraction (XRD), and *ex situ* synchrotron X-ray absorption spectroscopy. They found that the electrode is able to maintain the layered structure during the initial cycle. However, after a long period of cycling, the layered MnO_2 is completely transformed into spinel structure.[58] Zhou *et al.* investigated the energy storage process of MnO by inducing Mn defects to activate it, as shown in Figure 5E,F. During the charge and discharge processes, $Mn_{0.61}\square_{0.39}O$ provides more pathways for the diffusion of Zn^{2+} ions, thereby enhancing cyclic performance. The Zn^{2+} in $Mn_{0.61}\square_{0.39}O$ follows the insertion/extraction mechanism, preventing structural collapse of the material.[83]

3.2. Chemical Conversion Reaction. The mechanism of the chemical conversion reaction indicates that H^+ is involved in the charge−discharge process of MnO_2, resulting in the formation of a Zn basic complex in addition to the MnOOH phase. In 2016, Liu *et al.* found that a large and thick layer of flake-like basic zinc sulfate ($ZnSO_4[Zn(OH)_2]_3{\cdot}XH_2O$) was formed on the α-MnO_2 surface during the initial discharge, which could not be explained by the intercalation/de-intercalation mechanism of Zn^{2+}. Furthermore, they clarified that the capacity arose from the conversion reaction between MnO_2 and MnOOH. The X-ray diffraction (XRD) result further proved the coexistence of MnOOH and $Zn_4SO_4(OH)_6{\cdot}4H_2O$ after the initial discharge, as shown in Figure 6A,B. They proposed that MnOOH was formed by the reaction between α-MnO_2 and H^+ from the decomposition of H_2O in the electrolyte. With the increasing amount of MnOOH, the pH of electrolyte near the cathode surface gradually increased, causing the reaction of OH^- with Zn^{2+}, SO_4^{2-}, and H_2O, forming $ZnSO_4[Zn(OH)_2]_3{\cdot}XH_2O$. The reaction process is illustrated as follows:[95]

$$H_2O \leftrightarrow H^+ + OH^-$$

$$MnO_2 + H^+ + e^- \leftrightarrow MnOOH$$

$$\frac{1}{2}Zn^{2+} + OH^- + \frac{1}{6}ZnSO_4 + \frac{X}{6}H_2O \leftrightarrow \frac{1}{6}ZnSO_4[Zn(OH)_2]_3{\cdot}XH_2O$$

In addition, Kang *et al.* previously employed β-MnO_2 as the cathode materials for AZIBs. During the initial discharge, β-MnO_2 reacts with H^+ in water to form MnOOH, which is subsequently converted to Mn^{2+}. In subsequent cycles, the deposited MnO_2 reacts with H^+ to form MnOOH, accompanied by partial dissolution of Mn^{2+}, and simultaneous formation of $Zn_4SO_4(OH)_6{\cdot}5H_2O$ (Figure 6C,D). The reaction process is illustrated as follows:[96]

$$MnO_2 + H^+ + e^- \leftrightarrow MnOOH$$

$$MnOOH + 3H^+ + e^- \leftrightarrow Mn^{2+} + H_2O$$

$$4Zn^{2+} + SO_4^{2-} + 8H_2O \leftrightarrow Zn_4SO_4(OH)_6{\cdot}5H_2O + 6H^+$$

Liang *et al.* revealed a chemical conversion reaction mechanism. In the fully discharged state for the first time,

https://doi.org/10.1021/cbe.3c00120
Chem Bio Eng. 2024, 1, 113−132

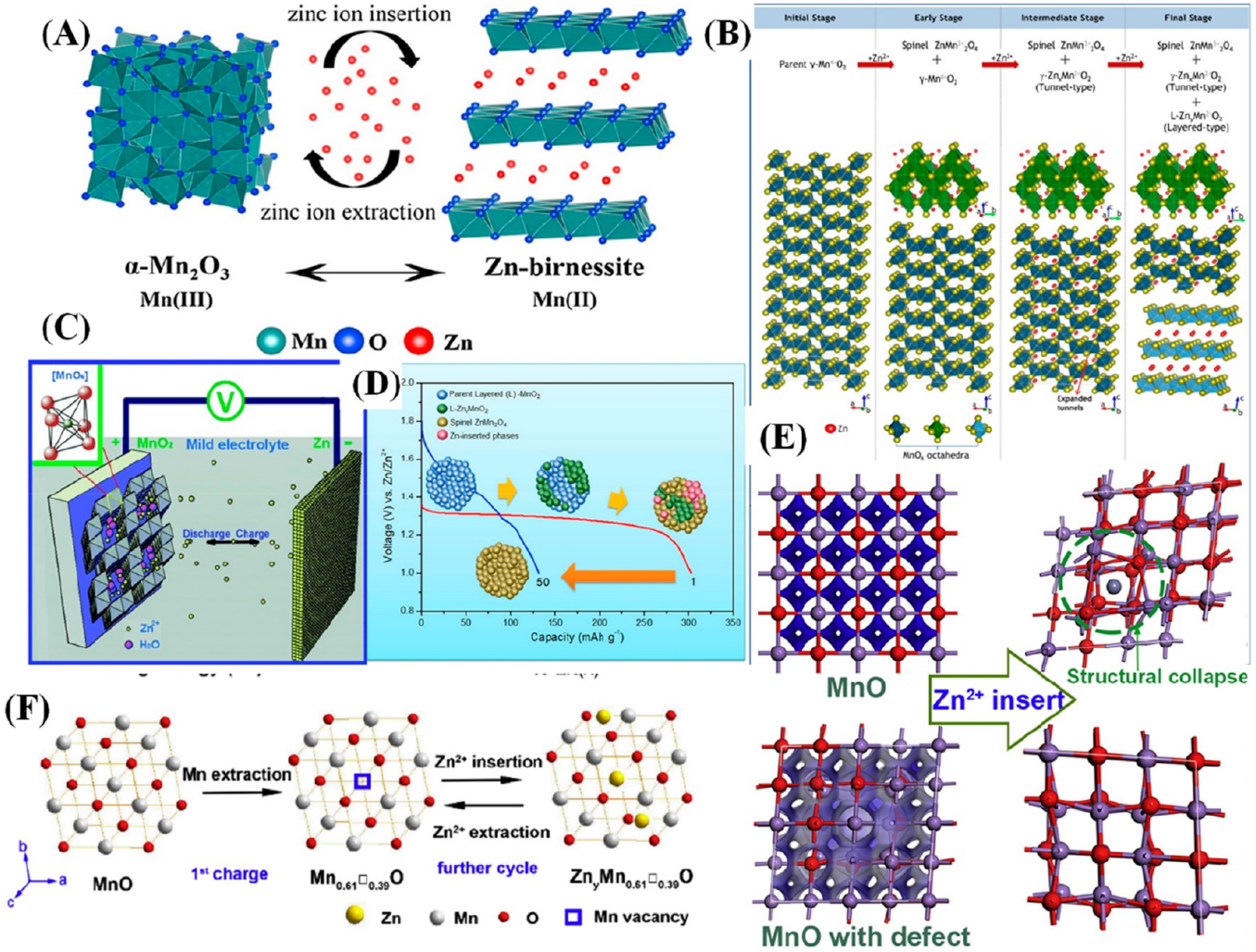

Figure 5. Reversible Zn insertion/extraction mechanism: (A) Schematics of manganese-based cathode materials as cathode material for zinc-ion battery. Reproduced with permission from ref 69. Copyright 2017, Elsevier. (B) Schematic representation of the reaction pathway for Zn insertion in γ-MnO_2 anode. Reproduced with permission from ref 94. Copyright 2015, American Chemical Society. (C) Schematics of the chemistry of the zinc-ion battery. Reproduced with permission from ref 32. Copyright 2012, Wiley-VCH. (D) Summary of Zn-ion insertion mechanism in layered MnO_2 structure. Reproduced with permission from ref 58. Copyright 2018, Elsevier. (E) Charge distribution of MnO and $Mn_{0.61}\square_{0.39}O$, and the structures after Zn^{2+} insert. Reproduced with permission from ref 83. Copyright 2019, Elsevier. (F) Schematic illustration of Zn^{2+} insertion/extraction in a MnO framework. Reproduced with permission from ref 83. Copyright 2019, Elsevier.

manganese(III) in Mn_3O_4 is reduced to manganese(II) in the form of MnO. $ZnSO_4$ and H_2O in the aqueous electrolyte react with subsequent OH^-, producing $ZnSO_4[Zn(OH)_2]_3{\cdot}5H_2O$. Upon complete charging, $ZnSO_4[Zn(OH)_2]_3{\cdot}5H_2O$ disappears, and Mn_3O_4 reappears, indicating the good reversibility for the electrode.[97]

3.3. Co-insertion/Extraction of H^+/Zn^{2+}. The discharge voltage profiles of aqueous Zn/MnO_x batteries exhibit two separated voltage plateaus, indicating two different electrochemical processes during discharge, in order to explain the two platforms that appeared at different voltages during the charge−discharge process of Zn/MnO_x batteries.[98] Pan *et al.* first proposed the H^+/Zn^{2+} co-insertion mechanism with MON ($MnO_2H_{0.16}(H_2O)_{0.27}$) as the positive electrode. The smaller radius of H^+ exhibits higher ion diffusion kinetics as compared to Zn^{2+} and hence is more favorable for de/insertion. Its schematic diagram is shown in Figure 7B.[99] Wang *et al.* proposed a novel reaction model of H^+/Zn^{2+} co-insertion/extraction by combining the mechanisms of Zn^{2+} insertion/extraction with conversion reaction, as shown in Figure 7A. Using galvanostatic intermittent titration technique (GITT) (Figure 7C), they found that the reaction kinetics of the first discharge platform were much faster than that of the second one.[100] Given the sluggish solid-phase diffusion induced by the high charge density and solvated structure of Zn^{2+}, together with the discharge products of MnOOH and $ZnMn_2O_4$ detected by *ex situ* XRD, they speculated that the rapid reaction kinetics for the first discharge platform were attributed to H^+ insertion, while the slow reaction kinetics for the second discharge platform originated from Zn^{2+} insertion. Furthermore, the second platform in the discharge curve of MnO_2 cathode is absent when operating in the electrolyte without $ZnSO_4$. The result further confirms the proposed mechanism of co-insertion/extraction of H^+/Zn^{2+}. Subsequently, Ji *et al.* found the identical behavior of H^+/Zn^{2+} co-insertion in α-MnO_2. Simultaneously, it was also found that the reversibility of H^+ storage is significantly higher than that of Zn^{2+} storage, and H^+ storage could stabilize the α-MnO_2 structure.[101] Yang *et al.* complements it by showing that intercalation and conversion reactions of H^+/Zn^{2+} occur at

https://doi.org/10.1021/cbe.3c00120
Chem Bio Eng. 2024, 1, 113−132

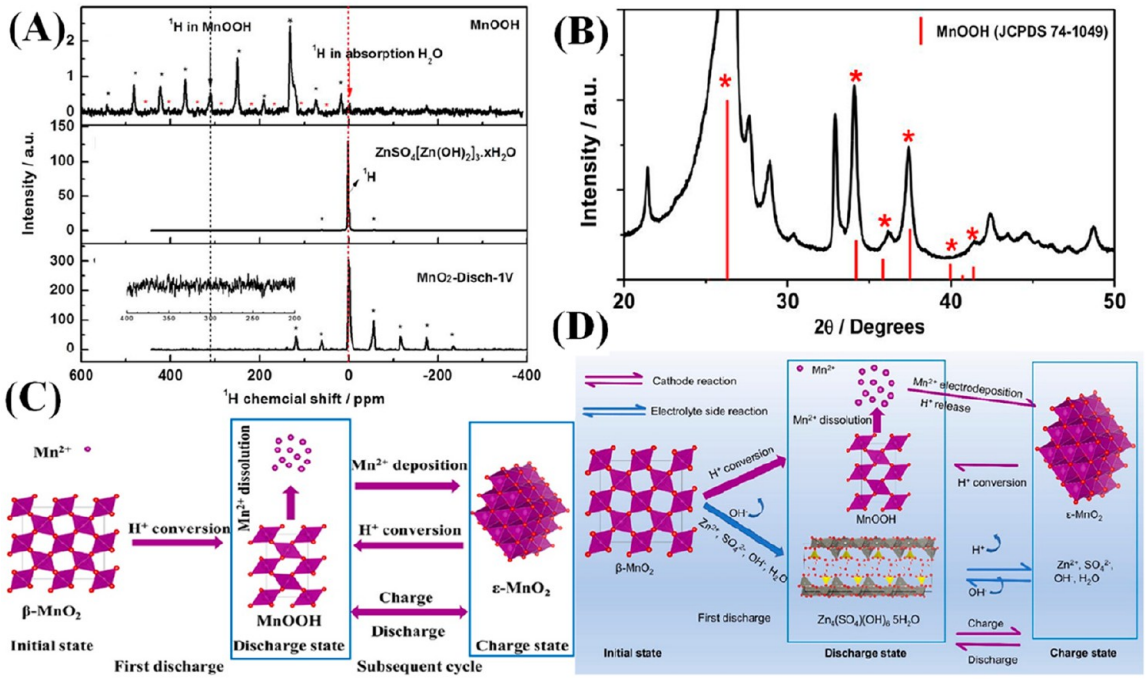

Figure 6. Chemical conversion reaction mechanism: (A) The solid state ^{1}H NMR (H Nuclear magnetic resonance) spectra MnOOH, $ZnSO_4[Zn(OH)_2]_3{\cdot}XH_2O$ and α-MnO_2 electrode discharged to 1 V (magic angle spinning at 35 kHz). Reproduced with permission from ref 95. Copyright 2016, Springer Nature Limited. (B) The XRD spectrum of the first discharge of α-MnO_2, where is the peak of MnOOH. Reproduced with permission from ref 95. Copyright 2016, Springer Nature Limited. (C) Schematics of β-MnO_2 as cathode material for zinc-ion battery. Reproduced with permission from ref 96. Copyright 2020, Science Press and Dalian Institute of Chemical Physics, Chinese Academy of Sciences. (D) Reaction pathways of β-MnO_2 during cycling. Reproduced with permission from ref 96. Copyright 2020, Science Press and Dalian Institute of Chemical Physics, Chinese Academy of Sciences.

different voltages and have different ion mobility rates at different voltages, as shown in Figure 7D,E.[102] Fenta *et al.* confirmed the presence of a reversible H^+/Zn^{2+} insertion/extraction mechanism in Cu-MnO·nH_2O through *in situ* techniques such as XRD, XPS, SEM, and STEM. The precipitation of MnOOH and ZHS occurs during the discharge process, while during the charging process, these precipitates disappear (Figure 7G).[103] Wang introduced the energy storage mechanism of MnO in ZIB (zinc-ion batteries), as shown in Figure 7F. During the initial charging process, the surface of MnO undergoes electrochemical oxidation to form MnO_2 nanosheets, becoming the active material for subsequent energy storage. In the following charge−discharge cycles, the activated MnO_2 undergoes two consecutive stages of reversible insertion/extraction of H^+ and Zn^{2+}.[104]

$$MnO_2 + H_2O + e^- \leftrightarrow MnOOH + OH^-$$

$$Zn^{2+} + 2MnO_2 + 2e^- \leftrightarrow ZnMn_2O_4$$

3.4. Dissolution/Deposition of Mn. The hydrogen-ion concentration (pH value) is also a very important factor that influences the performance of Zn−MnO_2 batteries. Typically, Mn^{2+} ions dissolve into the electrolyte with pH value increasing and recombine to the original structure when the pH value decreases. Zhi *et al.* reported a deposition−dissolution mechanism, as shown in Figure 8A. In an electrolyte containing Mn^{2+}, the deposition mechanism of MnO_2 is considered to be a multi-electron transfer process, following an electrochemical−chemical−electrochemical mechanism. The deposition process of MnO_2 involves three steps: Mn^{2+} is first electrochemically oxidized to Mn^{3+}, then Mn^{3+} is chemically converted to an intermediate product MnOOH, and finally, MnOOH is electrochemically oxidized to MnO_2. On the other hand, the dissolution mechanism of MnO_2 involves the electrochemical reduction of deposited MnO_2 to MnOOH, followed by its conversion to Mn^{3+}, and ultimately reduction to soluble Mn^{2+} ions. This entire process is accompanied by changes in proton concentration.[105] Kim *et al.* investigated the charge storage mechanism of $ZnMn_2O_4$, as shown in Figure 8B. They found that the main reason for the increased capacity of $ZnMn_2O_4$ material is the Mn^{2+} in the electrolyte, which contributes to the capacity through a quasi-reversible manganese deposition/dissolution process.[106]

In addition, Zhou *et al.* investigated the charge storage mechanism of two kinds of MnO_2 (α-MnO_2 and δ-MnO_2), as shown in Figure 8D,E.[107] They prepared a series of α-MnO_2 and δ-MnO_2 for aqueous Zn-ion batteries. They found the dissolution of Zn^{2+} of takes place between α-MnO_2 and H_2O, along with the release of OH^-, which will react with SO_4^{2-} and Zn^{2+} and then deposit on the surface of cathode materials to form the $Zn_4SO_4(OH)_6{\cdot}4H_2O$ (ZHS) phase. The result indicates the reaction mechanism of MnO_2 is based on the dissolution and deposition mechanism. The detail reaction mechanism is given below:

$$3MnO_2 + 6H_2O + 6e^- \leftrightarrow 3Mn^{2+} + 12OH^-$$

$$8Zn^{2+} + 2SO_4^{2-} + 8H_2O + 12OH^- \leftrightarrow 2Zn_4(OH)_6SO_4{\cdot}4H_2O$$

Oh *et al.* found a gradual increase in the pH of the electrolyte due to the disproportionation reaction of unstable

https://doi.org/10.1021/cbe.3c00120
Chem Bio Eng. 2024, 1, 113−132

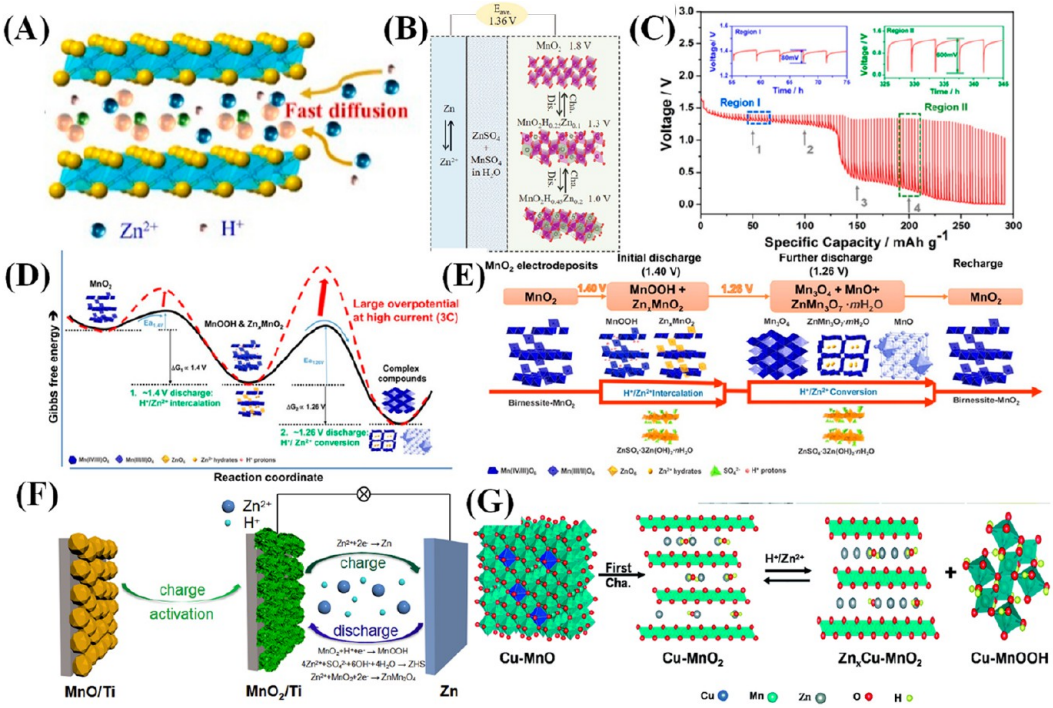

Figure 7. Co-insertion/extraction of H^+/Zn^{2+}: (A) Diagram of reaction of zinc-ion battery. Reproduced with permission from ref 81. Copyright 2019, American Chemical Society. (B) Diagram of structure of Zn/MON battery chemistry. Reproduced with permission from ref 99. Copyright 2019, WILEY-VCH. (C) GITT profile of Zn/MnO_2 @CFP (carbon fiber paper) cathode. Reproduced with permission from ref 100. Copyright 2017, American Chemical Society. (D) Schematic diagram of the thermodynamics and kinetics of redox reactions in Zn/MnO_2. Reproduced with permission from ref 102. Copyright 2019, American Chemical Society. (E) Schematic diagram of the crystal structure of the redox reaction of Zn/MnO_2. Reproduced with permission from ref 102. Copyright 2019, American Chemical Society. (F) A diagram of energy storage mechanism for the MnO cathode of ZIBs. Reproduced with permission from ref 104. Copyright 2019, Elsevier. (G) Schematics showing the phase transformation of Cu−MnO and the electrode reaction mechanism of Cu−$MnO_2{\cdot}nH_2O$. Reproduced with permission from ref 103. Copyright 2020, The Royal Society of Chemistry.

trivalent manganese during discharge and its dissolution in the electrolyte. This resulted in deposition of zinc hydroxide sulfate onto the electrode surface. During the charge process, the pH value of the electrolyte decreases due to recombination of manganese on the cathode, leading to dissolution of zinc hydroxide sulfate back into the electrolyte (Figure 8C).[82] Zhang and his co-workers revealed that the intercalation of Zn^{2+} in the δ-MnO_2 electrode is an ion-exchange process rather than an electrochemical process, and it does not affect the electrode's capacity. The research further elucidated that the electrochemical intercalation/deintercalation of H^+ in the δ-MnO_2 electrode, the electrochemical dissolution of δ-MnO_2, and the electrochemical dissolution−electrodeposition of hydrated birnessite play a predominant role in charge storage processes (Figure 8G).[108] Yang revealed the deposition/dissolution chemical properties of manganese dioxide in electrolytes with different proton concentrations, as shown in Figure 8H. The study found that during the deposition process, with an increase in proton concentration, Mn^{3+} gradually transforms into Mn(III) intermediates (MnOOH). In neutral electrolytes, only proton and metal ion intercalation reactions occur. In the dissolution process in acidic electrolytes, MnO_2 is first reduced to MnOOH instead of Mn^{3+}. However, with an increase in proton concentration, MnOOH cannot be fully reduced to Mn^{2+}. The dissolution of MnOOH and the disproportionation of Mn^{3+} lead to the formation of "dead" MnO_2.[109] Xu *et al.* proposed a $Zn_4SO_4{\cdot}(OH)_6{\cdot}xH_2O$ (ZSH) assisted deposition/dissolution model to elucidate the reaction mechanism of the aqueous Zn−MnO_x battery system, including MnO_2, Mn_2O_3, Mn_3O_4, and MnO. According to this model, the primary role of the MnO_2 cathode is to dissolve partially by consuming protons during the first discharge, inducing the formation of ZSH and releasing Mn^{2+} into the electrolyte. In subsequent cycles, the reversible capacity of the battery is mainly contributed by the ZSH-assisted Mn^{2+} deposition/dissolution reactions (Figure 8F).[110]

4. CHALLENGES AND MODIFICATIONS

The Mn-based oxides, recognized as promising cathode materials, have garnered extensive attention because of their low cost, high operating voltage, and high energy density. However, their practical application is impeded by several challenges, including the following.[111−114] (1) Inferior conductivity: Manganese-based materials exhibit semiconductor behavior with two types of charge carriers (electrons and holes) between the valence band and the conduction band, resulting in lower electrical conductivity. (2) Mn dissolution: The disproportionation reaction of Mn^{3+} leads to the dissolution of manganese in the form of Mn^{2+}, resulting in the loss of active material and contributing to poor structural and electrochemical stability in manganese-based materials. (3) Jahn−Teller (J-T) distortion: Manganese-based materials are formed by the aggregation of MnO_6 octahedra with shared corners/edges. The electric field present in MnO_6 leads to the separation of d orbitals, resulting in the formation of degenerate e_g orbitals (d_{z^2} and $d_{x^2-y^2}$) and t_{2g} orbitals (d_{xy},

https://doi.org/10.1021/cbe.3c00120
Chem Bio Eng. 2024, 1, 113−132

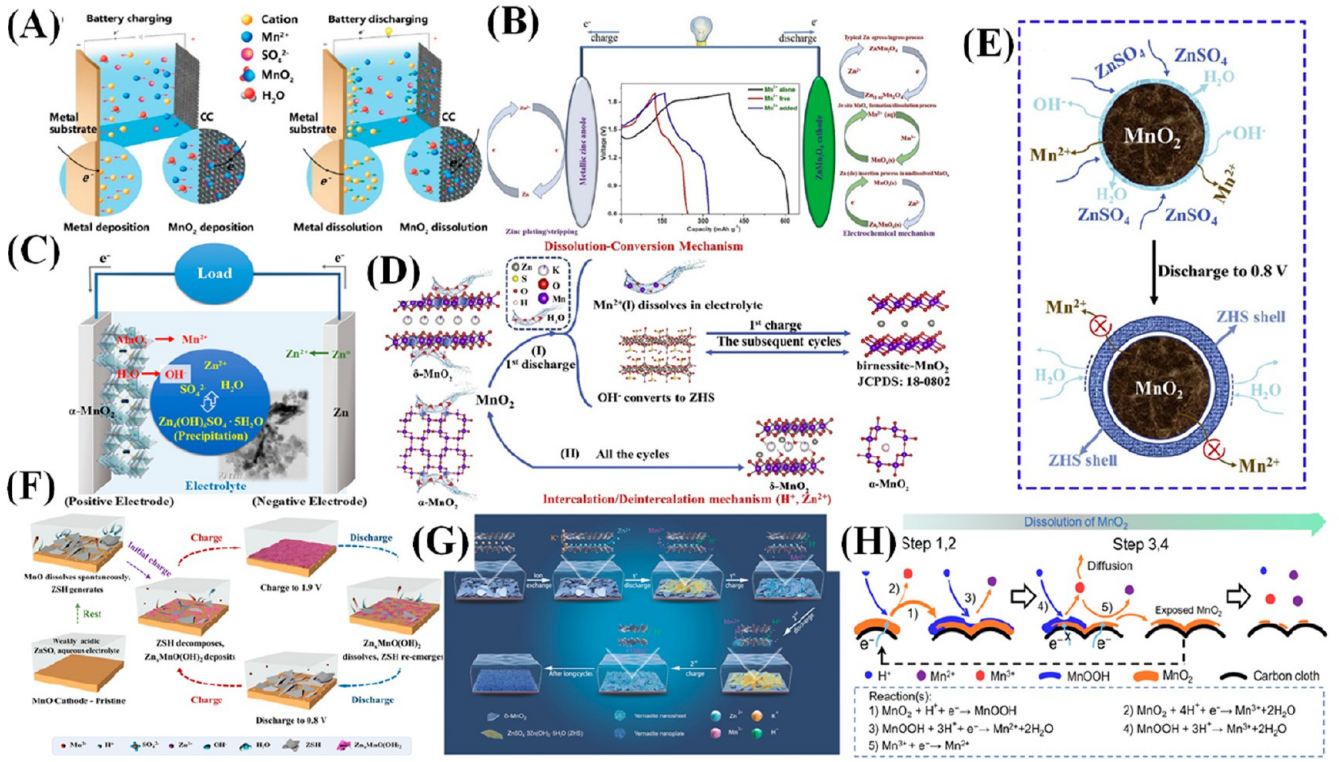

Figure 8. Dissolution/deposition of Mn: (A) Schematic illustration of the role of $Zn_4SO_4(OH)_6{\cdot}4H_2O$ in the discharge process. Reproduced with permission from ref 105. Copyright 2019, WILEY-VCH. (B) Schematic diagram of $ZnMn_2O_4$/Zn charging and discharging. Reproduced with permission from ref 106. Copyright 2019, Elsevier. (C) Schematics of α-MnO_2 as cathode material for zinc-ion battery. Reproduced with permission from ref 82. Copyright 2016, WILEY-VCH. (D) Schematic diagram of energy storage mechanism of Zn/MnO_2 battery. Reproduced with permission from ref 107. Copyright 2020, Elsevier. (E) Schematic diagram of the role of ZHS in the discharge process. Reproduced with permission from ref 107. Copyright 2020, Elsevier. (F) Illustration of the reaction mechanism for Zn−MnO battery in weakly acidic $ZnSO_4$ electrolyte. Reproduced with permission from ref 110. Copyright 2023, Elsevier. (G) Illustration of the reaction process of δ-MnO_2 electrode in AZIBs. Reproduced with permission from ref 108. Copyright 2024, WILEY-VCH. (H) Schematic of the dissolution of MnO_2 in acidic electrolytes. Reproduced with permission from ref 109. Copyright 2023, The Royal Society of Chemistry.

d_{xz}, and d_{yz}^2). In the high-spin state (e_g^1) of Mn^{3+}, the electron distribution is susceptible to disturbance, triggering the elongation of axial Mn−O bonds and the contraction of equatorial Mn−O bonds. This causes a distortion in the MnO_6 coordination from an octahedron to a distorted tetrahedron, known as the Jahn−Teller (J-T) effect. (4) Phase transition and collapse of crystal structure: During the deintercalation/intercalation discharge and charge processes of Zn^{2+}, manganese-based cathode materials undergo phase transitions. Transitioning from one phase to another or a combination of multiple phases results in lattice collapse and irreversible capacity loss. For instance, MnO_2 with a tunnel structure (α-MnO_2) during the discharge process can transform into a layered birnessite phase. The structural stress generated by the phase transition leads to the gradual breakdown of the original lattice structure, transitioning to an amorphous state, thereby causing capacity decay and deterioration in rate performance. (5) Sluggish diffusion kinetics of Zn^{2+}: Zn^{2+} exhibits a large solvated sheath and electrostatic repulsion due to its high charge/radius ratio, causing sluggish diffusion kinetics. Additionally, Zn ions can be solvated with H_2O molecules via hydrogen bonding to form large-radius hydrated Zn^{2+}, resulting in sluggish diffusion kinetics. (6) Insufficient active sites: The active sites within the bulk of the material remain unutilized, and during the Zn^{2+} adsorption process, strong electrostatic interactions induce a strong binding force between Zn atoms and O atoms, resulting in the irreversible loss of active sites. To address the aforementioned issues, various strategies have been implemented to improve electrochemical performance. These strategies include pre-intercalation, defect engineering, interface modification, morphology regulation, electrolyte optimization, composite construction, and activation of dissolution/deposition mechanisms.[27]

4.1. Pre-intercalation Strategy. Considering the lattice collapse and poor cycling performance of manganese-based cathode materials during cycles, researchers introduced guest molecules as "pillars" into the lattices to stabilize the structure of manganese-based cathode materials. These guest molecules serve as "pillars" to stabilize the main structure. Through the pre-intercalation strategy, general guest molecules, such as water molecules, metal cations, and organic molecules, are introduced into the main structure to achieve physical confinement. This helps alleviate issues related to volume change and structural collapse resulting from the repeated insertion/extraction of Zn^{2+} (Figure 9B). The introduction of crystal water can effectively shield the electrostatic interaction between Zn^{2+} and the crystal lattice, thereby promoting reaction kinetics. For instance, through the introduction of crystal water into the crystal lattice of MnO_2. Kim *et al.* discovered that the presence of crystal water in MnO_2 can enhance the capability for Zn storage, as shown in Figure 9A.[115] As the crystal water content increases, the cycle stability

https://doi.org/10.1021/cbe.3c00120
Chem Bio Eng. 2024, 1, 113−132

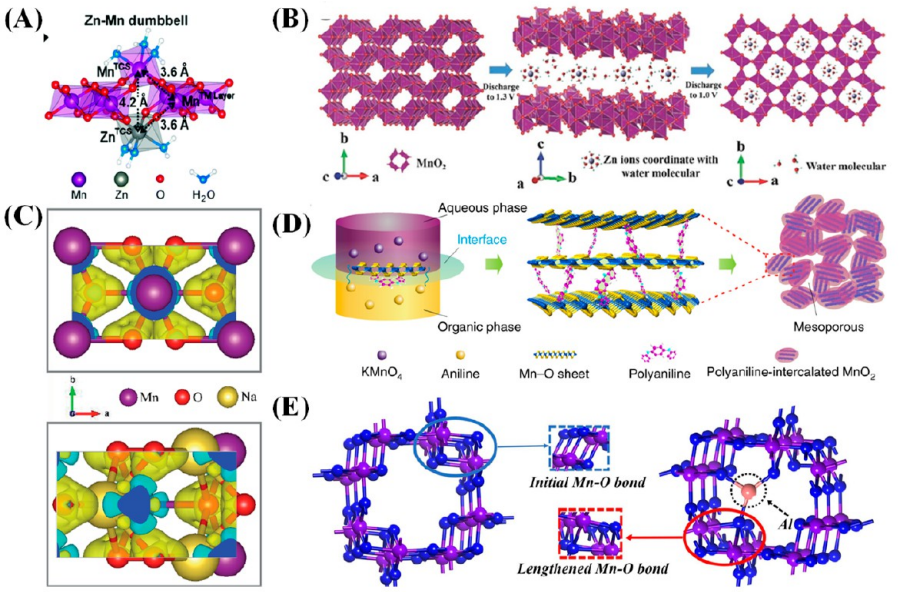

Figure 9. Pre-intercalation strategy: (A) DFT calculation of manganese dioxide electronic properties. Reproduced with permission from ref 115. Copyright 2019, Royal Society of Chemistry. (B) Schematic diagram of the intercalation mechanism. Reproduced with permission from ref 92. Copyright 2020, Science Press and Dalian Institute of Chemical Physics, Chinese Academy of Sciences. (C) Density functional theory calculations of the layered δ-MnO_2. Reproduced from ref 117 under at CC BY-NC 3.0 DEED. (D) Schematic illustration of expanded intercalated structure of polyaniline (PANI)-intercalated MnO_2 nanolayers. Reproduced with permission from ref 118. Copyright 2018, The Authors. (E) Structure diagrams of Al-intercalated MnO_2. Reproduced with permission from ref 116. Copyright 2021, Elsevier.

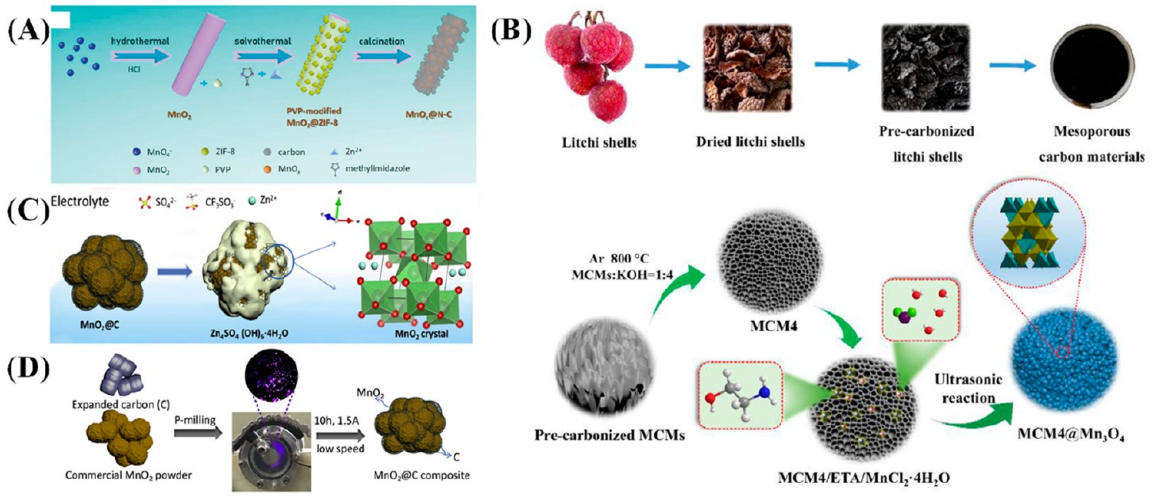

Figure 10. Surface modification: (A) Schematic illustration of MnO_x@N−C composites. Reproduced with permission from ref 86. Copyright 2018, WILEY-VCH. (B) Schematic diagram of the synthesis of MCM and MCM4@Mn_3O_4. Reproduced with permission from ref 120. Copyright 2020, Elsevier. (C) Schematic illustration of the reactions during the discharge process for β-MnO_2/Zn and (D) preparation processes of β-MnO_2@C composites. Reproduced with permission from ref 119. Copyright 2020, Elsevier.

of Zn/MnO_2 batteries also improves. The results indicate that both capacity and stability gradually increase with an increasing amount of crystal water. Furthermore, the crystal water in the layered structure contributes to the reduction of interfacial resistance and promotes diffusion kinetics for Zn ions. In addition, the insertion of metal cations can facilitate charge transfer of materials. For example, Yan *et al.* investigated the effect of Al^{3+} intercalation on MnO_2 cathode material, revealing that the inserted Al^{3+} could form a stable Al−O bond in the tunnel-type MnO_2 skeleton, as shown in Figure 9E. This bond could regulate the charge/ion states and electronic band gap, improve the reversibility of the phase transition for the cathode, and reduce the tendency of Mn^{2+} dissolution.[116] As illustrated in Figure 9C, Fan *et al.* introduced Na^+ into the layer of δ-MnO_2. The results show that the MnO_2, after the introduction of Na^+, has high capacity, high energy density, and excellent cycling stability. This is due to the enhancement of ionic conductivity by the insertion of Na^+ into the middle layer of the host material.[117] Comparatively, large-sized polymers can further expand the layer spacing to accelerate ion diffusion kinetics. For example, Wang *et al.* developed the PANI (polyaniline) intercalated MnO_2, with an expanding layer spacing of ∼1.0 nm. Simultaneously, the phase transition and structural collapse of MnO_2 could also be

https://doi.org/10.1021/cbe.3c00120
Chem Bio Eng. 2024, 1, 113−132

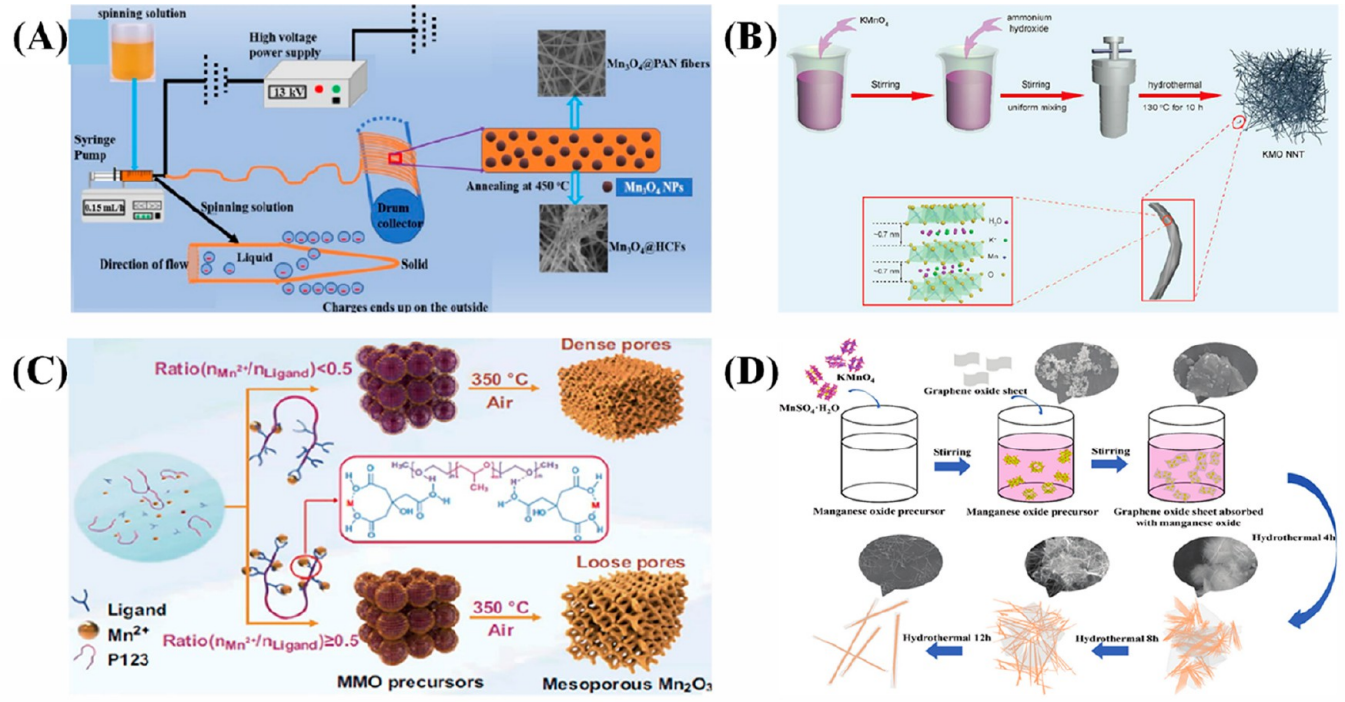

Figure 11. Special morphology regulation: (A) Schematic of preparing process of the Mn_3O_4@HCFs. Reproduced with permission from ref 123. Copyright 2020, Elsevier. (B) Schematic illustration of the synthesis of 1D K^+-inserted δ-MnO_2 nanowires. Reproduced with permission from ref 122. Copyright 2021, Elsevier. (C) Schematic diagram of mesoporous Mn_2O_3 synthesis. Reproduced with permission from ref 124. Copyright 2019, The Authors. (D) Schematic illustration of the formation of the α-MnO_2/graphene scrolls. Reproduced with permission from ref 76. Copyright 2018, WILEY-VCH.

inhibited. As a result, prolong cycle life of Zn/MnO_2 batteries are obtained (Figure 9D).[118] The pre-intercalation strategy can improve the structural stability of the material. However, the ions pre-intercalated partially occupy the diffusion pores, resulting in negative effects on the diffusion efficiency of Zn^{2+}. Additionally, the influence of hydrogen bonds that exist between crystal water or organic molecules and MnO_2 on the structure of modified materials remains unclear.

4.2. Surface Modification Strategy. The manganese-based cathode material itself has poor electronic conductivity, impeding the embedment and removal of ions in the lattice and the dissolution of manganese. Therefore, coating the Mn-based oxides with materials possessing good conductivity (*e.g.*, carbons, graphene, carbon nanotubes, polymers, and metal−organic frameworks, etc.) via interface modification has been proposed to enhance the electronic conductivity and discharge capacity of matrixes. This approach simultaneously suppresses the dissolution of active materials. For example, Hu *et al.* reported a plasma-treated β-MnO_2@C cathode material for aqueous Zn/MnO_2 batteries, as shown in Figure 10C,D. The carbon coating resulted in improved electrochemical performance (maintaining a capacity retention of 100% after 400 cycles).[119] As illustrated in Figure 10A, Sun *et al.* successfully prepared the metal−organic-framework-derived and carbon-coated MnO_x@N−C (N-doped carbon and amorphous carbon-coated MnO_x nanorods) with porous skeleton as cathode material for application in the aqueous zinc-ion battery.[86] Benefiting from its distinct porous structure, the electrochemical performance was improved due to the excellent conducting networks (high capacity of 305 mAh g^{-1} after 600 cycles at 500 mA g^{-1}). Additionally, polymer coatings have also been proven effective for the modification of Mn-based oxides. After high-temperature heat treatment, a shell of heteroatom (N, S, etc.)-doped carbon material with better chemical performance will be formed on polymer-coated Mn-based material. For example, Liu *et al.* incorporated Mn_3O_4 composite into the pores of mesoporous carbon. The effective coordination of Mn_3O_4 and MCM4 (mesoporous carbon materials) facilitates the improvement of ion transport kinetics and the enhancement of electronic conductivity. This results in excellent cycling performance of MCM4@Mn_3O_4 (Mn_3O_4 particles were coated on the surface of MCM4), and the capacity decay rate of MCM4@Mn_3O_4 is significantly lower than that of pure Mn_3O_4 electrode (Figure 10B).[120]

4.3. Nanostructured Electrode Materials Design. Designing nanostructured electrode materials (such as hollow, core−shell, and porous, etc.) is also an effective strategy to improve the properties of manganese-based cathode materials. The hollow core−shell structure can not only shorten the diffusion path of Zn^{2+} but also alleviate the volume expansion of the material during the cycling process, thus improving the rate performance and cycle stability of zinc-ion batteries. Generally, porous nanomaterials have a large specific surface area, enabling the exposure of more redox-active sites and thereby improving reversible specific capacity. For example, Guo *et al.* investigated the effects of MnO_2 with varying morphologies on battery performance, declaring that MnO_2 nanorods delivered inferior cycling performance with rapid capacity fading. Meanwhile, MnO_2 with a hollow nanosphere morphology could buffer the stress caused by Zn^{2+} insertion/extraction, exhibiting excellent rate performance and cycling stability.[121] In addition, the diffusion paths of Zn ions will be shortened in nanostructured composites. The connection between nanowires can facilitate electron and ion transport.

https://doi.org/10.1021/cbe.3c00120
Chem Bio Eng. 2024, 1, 113−132

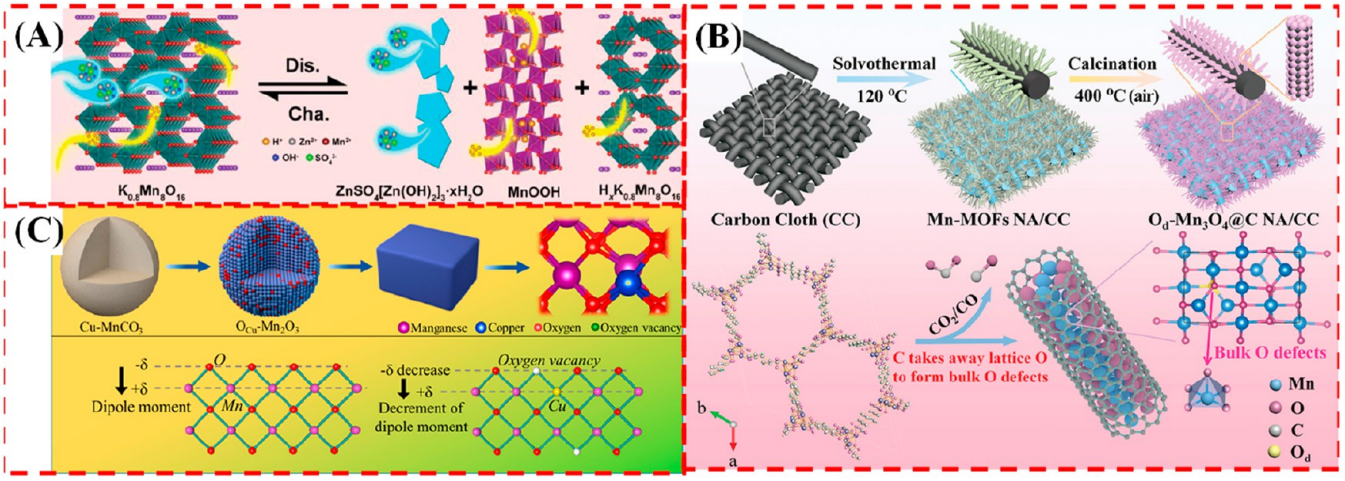

Figure 12. Defect engineering: (A) Schematic diagram of the electrochemical reaction mechanism of zinc-ion battery. Reproduced with permission from ref 126. Copyright 2019, WILEY-VCH. (B) Schematic diagram of the synthesis of oxygen deficient Mn_3O_4. Reproduced with permission from ref 127. Copyright 2020, WILEY-VCH. (C) Schematic illustration of O_{cu}-Mn_2O_3. Reproduced with permission from ref 128. Copyright 2020, American Chemical Society.

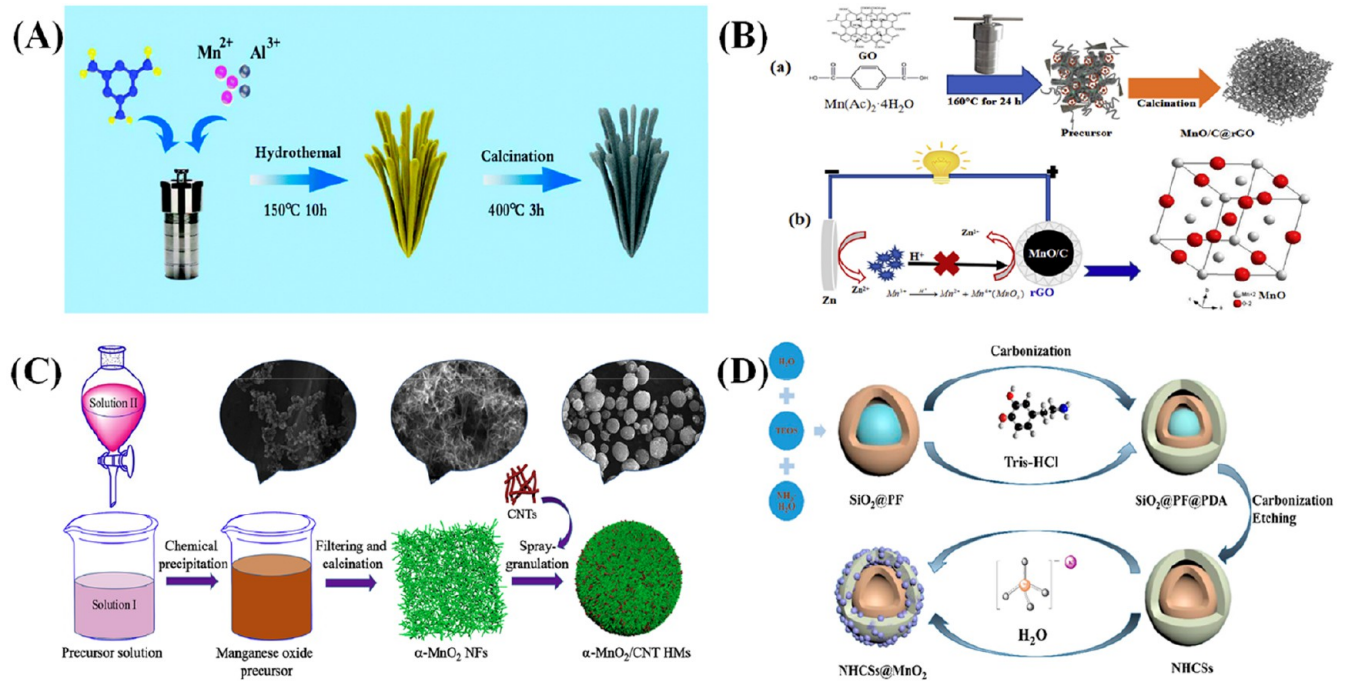

Figure 13. Composite construction: (A) Schematic illustration of the formation of the Mn_2O_3/Al_2O_3 composite. Reproduced with permission from ref 130. Copyright 2019, Royal Society of Chemistry. (B) Schematic diagram of MnO/C@rGO synthesis and manganese dissolution mechanism. Reproduced with permission from ref 131. Copyright 2020, Elsevier. (C) Schematic diagram of preparation of α-MnO_2/CNT and corresponding SEM diagrams. Reproduced with permission from ref 132. Copyright 2019, Elsevier. (D) Schematic diagram of NHCSs@MnO_2 (grown MnO_2 particles on the surface of N-doped hollow porous carbon nanospheres) composite material synthesis. Reproduced with permission from ref 133. Copyright 2020, Elsevier.

Li *et al.* prepared a series of 3D δ-MnO_2 nanowires for Zn-ion batteries, as shown in Figure 11B.[122] Owing to the unique 3D structure, excellent electrochemical performance is obtained. As illustrated in Figure 11D, Mai *et al.* prepared a cathode material by coating graphene rolls with α-MnO_2 nanowires.[76] The graphene coating not only improves the conductivity of the cathode materials but also suppresses the dissolution of Mn^{2+} into the electrolyte. Owing to the unique 3D structure, the material has a high energy density (0.3 A g^{-1}, 382.2 mAh g^{-1}) and good long-cycle stability (94% capacity retention after 3000 cycles at 3 A g^{-1}). Yang *et al.* also prepared a Mn_3O_4@HCFs (Mn_3O_4 nanoparticles in the hollow carbon fibers) with core−shell structure via coaxial electrospinning (Figure 11A).[123] This core−shell structure exhibit long-term cycle stability over 1300 times with a capacity retention over 96% under the current rate of 400 mA g^{-1}. As shown in Figure 11C, Qiao *et al.* synthesized porous nanostructured Mn_2O_3 for Zn/Mn_2O_3 batteries. Zn//Mn_2O_3 exhibits excellent rate performance and cycle stability due to its nanoporous structure. The Mn_2O_3 electrode demonstrates high reversible capacity (233

https://doi.org/10.1021/cbe.3c00120
Chem Bio Eng. 2024, 1, 113−132

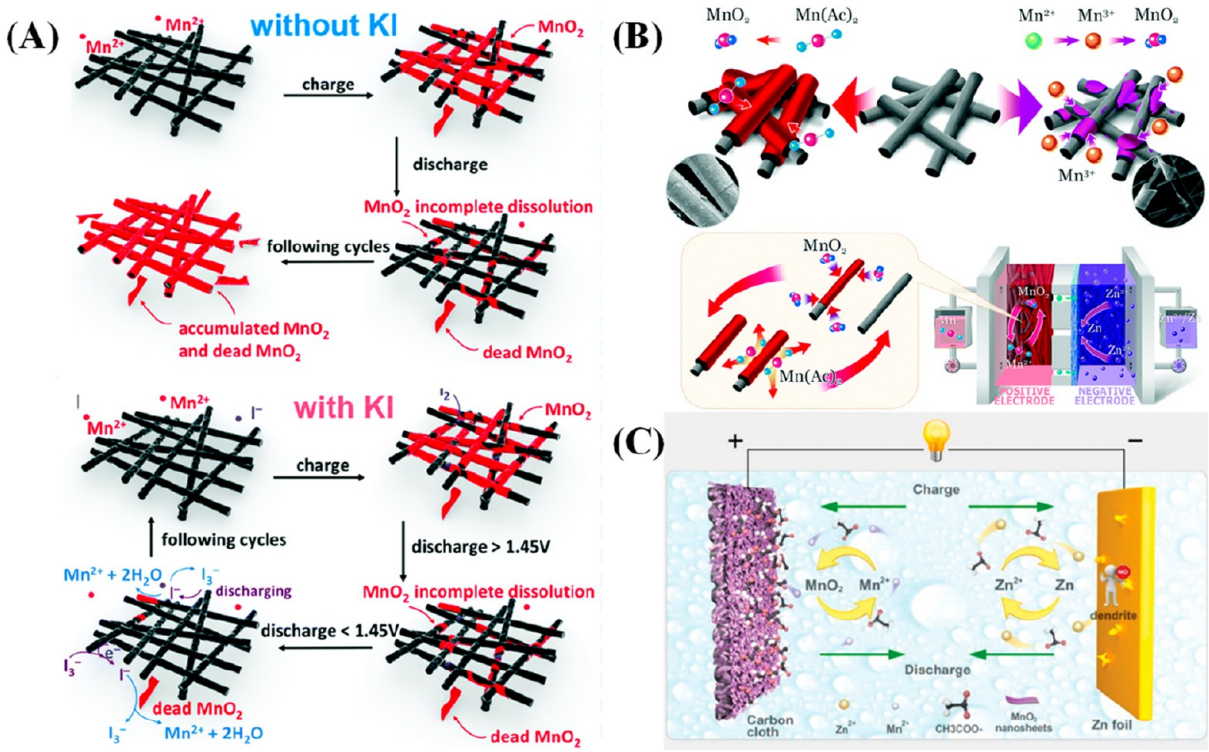

Figure 14. Activation of dissolution/deposition mechanism: (A) Schematic diagram of the electrochemical process of manganese cathode. Reproduced with permission from ref 134. Copyright 2021, Royal Society of Chemistry. (B) Electrochemical mechanism of the Mn $(Ac)_2$ and $MnSO_4$ electrolyte. Reproduced with permission from ref 135. Copyright 2020, Royal Society of Chemistry. (C) Schematic illustration of the aqueous rechargeable Zn/MnO_2 energy storage system in the acetate-based electrolyte. Reproduced with permission from ref 79. Copyright 2020, WILEY-VCH.

mAh g^{-1} at 0.3 A g^{-1}) and superior rate capability (162 mAh g^{-1} retains at 3.08 A g^{-1}).[124]

4.4. Defect Engineering. In recent years, defect engineering of material structures has been widely used to improve the electrochemical properties of manganese-based materials. Defects in materials can be categorized into the following four groups: (1) point defects (*e.g.*, vacancies and doping), (2) line defects (*e.g.*, dislocations), (3) plane defects (*e.g.*, grain boundaries), and (4) bulk defects (*e.g.*, spatial lattice disorders). Among them, oxygen vacancy, as a common structural modification strategy, has been applied for the modification of Mn-based materials.[52] Xue *et al.* artificially built the oxygen vacancy (Od-MnO_2) in the MnO_2 cathode to improve its electrochemical performance. The calculation results showed that the Gibbs adsorption free energy of Zn^{2+} changed from −3.31 to +0.05 eV after the introduction of oxygen vacancy, which was close to the thermal neutral value. This led to the reinforced reversible adsorption/desorption capacity of Zn^{2+}, which was helpful in improving the utilization rate of the material, presenting a higher contribution of surface capacitance.[125] For example, Zhou *et al.* introduced K^+ into the oxygen vacancy of MnO_2 for aqueous Zn-ion batteries, as shown in Figure 12A. Owing to the presence of K^+ in the oxygen vacancy, improved rate capability can be achieved (a significant energy output of 398 Wh kg^{-1} and a long-term cycle life up to 1000 cycles).[126] Tan *et al.* studied Mn_3O_4@C nanorods with oxygen deficiencies. Oxygen deficiency can stabilize (MnO_6) octahedral structure and inhibit the dissolution of Mn^{2+}. The presence of an oxygen vacancy effectively suppresses the dissolution of Mn^{2+} into the electrolyte (Figure 12B).[127] Liang *et al.* prepared a N−Vo−MnO_{1-x} (melamine mixed with MnO) cathode by introducing both nitrogen doping and oxygen vacancy into low-valence MnO. The nitrogen doping improved the intrinsic conductivity of MnO, while the oxygen vacancy not only increased the storage sites of Zn^{2+} but also released the stress generated during the continuous insertion/extraction of Zn^{2+}, resulting in satisfactory rate and cycling performance for the N−Vo−MnO_{1-x} cathode.[72] In addition, Zhang *et al.* synthesized oxygen-defective manganese-based cathode material by doping low-valence Cu ions (O_{cu}−Mn_2O_3). The presence of an oxygen defect modifies the internal electric field of the material and enhances the substantial electrostatic stability by compensating for the nonzero dipole moment (Figure 12C).[128]

4.5. Composite Construction. Composite materials, consisting of two or more components, have been proposed to take advantage of the synergistic effect between different components. From the perspective of structural optimization, composite construction is effective in improving the overall performance of the electrode. Chen *et al.* fabricated hierarchical porous nanorods made up of α-(Mn_2O_3−MnO_2) heterostructures, resulting in improved interfacial reaction kinetics and strengthened charge transport due to their distinct morphology, along with the formed internal electric field at the heterojunction interface. As a result, the α-(Mn_2O_3−MnO_2) cathode could still deliver a discharge capacity of 170 mAh g^{-1} after 2000 cycles at 500 mA g^{-1}.[129] In addition, Gou *et al.* prepared Mn_2O_3/Al_2O_3 composites by employing metal−organic frameworks as precursors, as shown in Figure 13A. The

https://doi.org/10.1021/cbe.3c00120
Chem Bio Eng. 2024, 1, 113−132

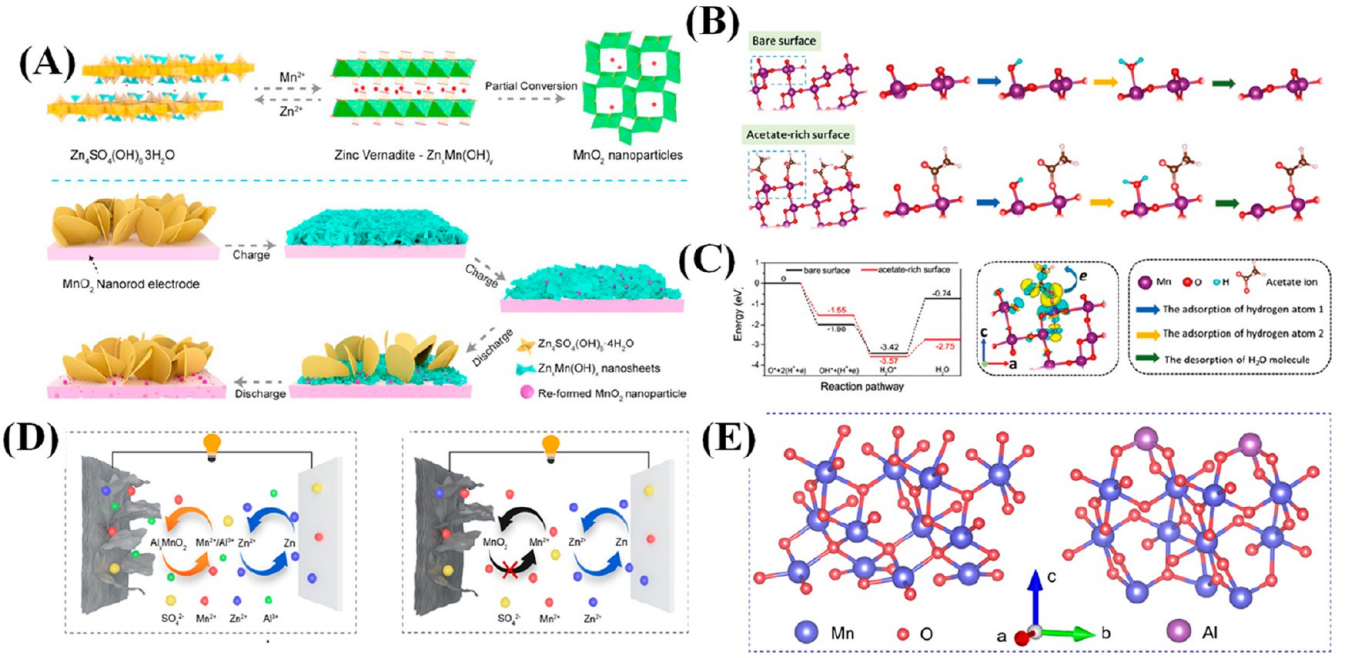

Figure 15. Electrolyte optimization: (A) Schematic diagram of the phase transition and structural evolution during continuous electrochemical conversion reactions. Reproduced with permission from 140. Copyright 2021, Elsevier. (B) Atomic structure of the dissolution reaction on the bare surface and acetate-rich surface of MnO_2. Reproduced with permission ref 79. Copyright 2020, WILEY-VCH. (C) Energy diagram of the dissolution reaction on the bare surface and acetate-rich surface of MnO_2, along with the charge density difference of acetic acid ions adsorbed on MnO_2, where yellow and blue represent the electron accumulation region and depletion region, respectively. Reproduced with permission from ref 79. Copyright 2020, WILEY-VCH. (D) Schematic illustration of the aqueous Zn−(Al)Mn and Zn−Mn hybrid batteries, respectively. Reproduced with permission from ref 141. Copyright 2022, American Chemical Society; (E) Crystal structures of MnO_2 and $Al_{0.2}MnO_x$, respectively. Reproduced with permission from ref 141. Copyright 2022, American Chemical Society.

dissolution of Mn^{2+} can be suppressed by this strategy. Compared with pristine Mn_2O_3, the modified cathode material exhibits higher discharge specific capacity and improved cycle stability (118 mAh g^{-1} discharge specific capacity after 1100 cycles at 1500 mA g^{-1}).[130]

Moreover, Tang *et al.* prepared MnO/C@rGO (carbon-coated graphene (GO) and MnO composites) composites via the solvothermal method. The prepared MnO/C@rGO can effectively suppress Mn^{2+} dissolution and improve conductivity of MnO. As a result, the material has excellent cycle stability and rate performance and small self-discharge phenomenon. Even at a high current density of 2.0 A g^{-1}, the material still exhibits a high discharge specific capacity of 110.1 mAh g^{-1} (Figure 13B).[131] Moreover, as shown in Figure 13C, Chi *et al.* employed α-MnO_2/CNT HMs (α-MnO_2 nanofiber/carbon nanotube composites). Owing to the unique morphology of α-MnO_2/CNT HMs, the composite exhibits high tap density and high electrical conductivity. As a result, Zn/MnO_2 batteries with an α-MnO_2 nanofiber/carbon nanotube composite cathode exhibit high area energy density of 0.98 Wh cm^{-2} and good cycle retention (96% capacity retention at 3 A g^{-1} cycle).[132] Finally, Kong *et al.* prepared a composite of hollow carbon material combined with MnO_2, as shown in Figure 13D. Hollow porous carbon nanostructures enable cathodes with larger electron-modified interfaces, higher loadings, and stable structures. Hence, even at a current density of 500 mA g^{-1}, the Zn/MnO_2 batteries still show improved discharge specific capacity (103 mAh g^{-1}) and cycle retention rate (98.3% after 650 cycles).[133]

4.6. Activation of Dissolution/Deposition Strategy. Since the capacity attenuation of manganese-based oxide electrode materials is mainly derived from structural collapse and Mn dissolution, some researchers have proposed fully activating the deposition/dissolution mechanism of manganese-based oxides through the rational design of electrolyte and regulation of charge/discharge intervals. Compared with the aforementioned strategies, the dissolution/deposition mechanism can fundamentally address the issue of capacity attenuation, entirely avoiding structural collapse. Lu *et al.* propose a mediator strategy to improve cycling stability at high area capacity. The chemical reduction of MnO_2 to produce Mn^{2+} via the iodide (I^-) medium and oxidizing it to triiodide (I^{3-}), which is then reduced to I^- at the electrode to facilitate dissolution of manganese dioxide and to recover the "lost" capacity from stripped manganese dioxide. This work demonstrates that the use of a readily soluble mediator strategy can unlock the high area capacity of manganese-based cells with a deposition−dissolution reaction mechanism and show superior cycling stability (Figure 14A).[134] Li *et al.* proposed a reversible Mn^{2+}/MnO_2 redox couple with high stability for the first time. Through the coordination effect of Ac^-, Mn^{2+} can be directly deposited on the electrode as MnO_2. Compared with the common intercalation mechanism, the dissolution/deposition reaction completely avoids structural collapse and improves the stability of the cathode. In addition, problems caused by Mn^{3+} disproportionation can be avoided compared to Mn^{3+}/Mn^{2+} redox (Figure 14B).[135] Finally, Guo *et al.* proposed a strategy for a neutral acetate-based electrolyte (pH ≈ 6) to promote the Mn^{4+}/Mn^{2+} redox reaction, as shown in Figure 14C. The Zn/MnO_2 battery exhibits excellent discharge specific capacity (556 mAh g^{-1}), cycle stability (4000

https://doi.org/10.1021/cbe.3c00120
Chem Bio Eng. 2024, 1, 113−132

cycles without attenuation), and excellent rate performance (70 mA cm^{-2}).[79]

4.7. Electrolyte Optimization. Due to the disproportionation reaction of Mn^{3+} and the Jahn−Teller effect causing the loss of active material, manganese-based materials exhibit poor structural and electrochemical stability.[136] To mitigate manganese dissolution, adding Mn^{2+} to the electrolyte or using alternative electrolytes such as $Zn(CF_3SO_3)_2$ or $Zn(CH_3COO)_2$ instead of $ZnSO_4$ can effectively prevent manganese dissolution. The addition of Mn^{2+} effectively inhibits the dissolution of MnO_2, thereby reducing the Mn vacancies generated by Zn^{2+} insertion.[137,138] To some extent, this stabilizes the crystal structure, reduces the formation of poorly electrochemically active spinel phase $ZnMn_2O_4$, and improves the cyclic stability of the electrode. Additionally, the inclusion of manganese salts can partially suppress the increase in the oxygen evolution reaction potential and broaden the electrochemical stability window of water.[139]

In 2016, Pan *et al.* addressed the issue of manganese dissolution causing the loss of active material in manganese oxide cathode materials. They proposed the addition of a small amount of manganese salts to the electrolyte to mitigate this problem. They found that the presence of a certain amount of Mn^{2+} in the electrolyte inhibits the disproportionation reaction of discharge product Mn(III), thereby suppressing manganese dissolution.[95] As shown in Figure 15A, Bao *et al.* added a certain amount of Mn^{2+} to the electrolyte, the battery can improve the capacity and cycling abilitily through converted electrodepostion of Mn^{2+}. During the charging process, $Zn_4SO_4{\cdot}(OH)_6{\cdot}4H_2O$ can generate $Zn_xMnO(OH)_y$, which then regenerates $Zn_4SO_4{\cdot}(OH)_6{\cdot}4H_2O$ during the discharging process. Additionally, when the charging voltage for Zn/Zn^{2+} exceeds 1.6 V, some zinc vernadite nanosheets irreversibly transform into tunnel-like MnO_2 nanocrystalline material, enhancing the specific capacity of Zn/MnO_2 batteries in subsequent cycles. This results in excellent cycling stability for Zn/MnO_2 batteries.[140] Guo *et al.* found that acetate ions in the electrolyte can alter the surface properties of manganese dioxide cathodes and reduce barriers in the dissolution process (Figure 15B,C). Additionally, they stimulate the Mn^{4+}/Mn^{2+} redox reaction, which, compared to the traditional Mn^{4+}/Mn^{3+} redox reaction, exhibits higher capacity and better cyclic reversibility. Furthermore, the nearly neutral acetate-based electrolyte ensures excellent stability and compatibility for the zinc anode, resulting in a higher electroplating/stripping Coulombic efficiency for the zinc anode.[79] Liu prepared a feasible $Zn-MnO_2$ hybrid aqueous battery by adding $Al_2(SO_4)_3$ to the $ZnSO_4$ + $MnSO_4$ electrolyte, as depicted in Figure 15D,E. On one hand, the aqueous Al^{3+} acts as a proton to maintain an acidic environment near the surface of the $Al_{0.2}MnO_x$ cathode, preventing the formation of $Zn_4(OH)_6(SO_4){\cdot}0.5H_2O$ during discharge. On the other hand, the introduction of Al^{3+} during the charging process introduces numerous oxygen vacancies into the oxide structure ($Al_{0.2}MnO_x$) and weakens the Mn−O bonds. These effects facilitate the dissolution reaction of the manganese oxide cathode. Therefore, the Zn−(Al)Mn hybrid battery exhibits excellent electrochemical performance, including high discharge capacity (564.7 mAh g^{-1}) and long cycle life (2000 cycles).[141] The concentration of Mn^{2+} has a significant impact on both the capacity and stability. As the concentration of Mn^{2+} gradually increases in the electrolyte, the capacity initially reaches its maximum value and then gradually decreases. Additionally, manganese salts in the electrolyte can deposit as manganese oxide. The deposited manganese oxide can also serve as an active material, potentially causing inaccuracies in the actual capacity of the manganese oxide cathode. This may mislead certain comparisons of manganese oxide performance, rendering them meaningless.

5. SUMMARY AND OUTLOOK

Due to their cost-effectiveness, environmental friendliness, good safety, and relatively high capacity, aqueous zinc-ion batteries are promising for practical applications in large-scale energy storage. Based on the features of Mn-based oxide cathode materials, this paper has outlined the development history and research progress of Mn-based oxide cathode materials, as well as clarified the energy-storage mechanism of Mn-based oxide cathode materials. In addition, the mechanisms and research status of modification strategies, including pre-intercalation, defect engineering, electrolyte optimization, and activation of the dissolution/deposition mechanism, have been presented. While manganese-based oxide cathode materials have been explored for a considerable period, achieving commercial applications still requires further research to address some key issues. Based on our analysis, the future research directions for AZIBs (aqueous zinc-ion batteries) are envisioned in the following aspects:

(1) Developing new coating materials. New coating materials, such as polymer materials with features like uniform active sites, good conductivity, and hydrophilicity, can effectively improve the electrochemical performance for the electrodes. Additionally, exploring the synergistic effects between multicomponent coating materials is worth further investigation. For instance, a bilayer coating composed both of an electronic and ion conductor layer can effectively suppress surface side reactions and enhance the conductivity of manganese-based oxide cathode materials. Moreover, the coating layers also help in providing a uniform electric field to inhibit dendritic growth of the zinc anode.

(2) Exploring new electrolyte additives. Electrolyte additives can not only regulate the deposition of zinc ions on the surface of the zinc anode but also act on the cathode interface to enhance the cyclic stability of the cathode material. Developing hydrophilic electrolyte additives is also a promising strategy as it can effectively immobilize free water molecules and further suppress the surface side reactions. The functionality of a single electrolyte additive is relatively limited, combining the multiple effects of electrolyte additives may also lead to optimal performance.

(3) Electronic structure modulation. Improving the electronic structure of materials in terms of metal-ion oxidation states, atomic coordination environments, charge density distribution, and band structure is achieved through calculations involving band structures, Fermi levels, density of states (DOS), and lattice stress. This electronic structure modulation aims to enhance the number of active sites, stabilize lattice structures, suppress Jahn−Teller distortions, improve ion diffusion kinetics, enhance material conductivity, reduce ion transport barriers, accelerate ion desorption, and establish internal electric fields. These measures collectively contribute to enhancing the electrochemical

https://doi.org/10.1021/cbe.3c00120
Chem Bio Eng. 2024, 1, 113−132

performance of manganese-based oxide cathode materials.

(4) Investigating the byproducts and intermediate products. During the electrochemical reaction process, a series of byproducts are formed on the cathode surface. These byproducts can have a significant impact on battery performance, affecting the transfer of electrons and ions, limiting battery capacity, and even altering reaction mechanisms. However, the current attention to the intermediate products generated during the reaction process is far from sufficient. Effective strategies to address the battery failure caused by these intermediate products are still lacking. There is also no unified consensus on the types, structures, and influencing factors of these intermediate products. Therefore, future research should focus on more investigating the byproducts and intermediate products generated during electrochemical reactions.

(5) Suppressing active water molecules in solid/gel polymer electrolytes. Solid/gel polymer electrolytes have a strong affinity for free water, which can effectively slow down the dissolution of zinc dendrites and Mn disintegration. Therefore, it is crucial to design solid/gel polymer electrolytes with high ion conductivity, excellent mechanical durability, good interface contact with electrodes, high Zn^{2+} migration rate, and a broad electrochemical and thermal stability window. Additionally, further exploration of new polymer matrixes and zinc salts for solid/gel polymer electrolytes, or modifying specific properties of solid/gel polymer electrolytes through methods like copolymerization, composite formation, or adding functional groups, is necessary. This is essential for the future application of AZIBs in wearable and portable electronic devices.

(6) Exploring mechanisms, optimizing for application, and cost/profit analysis. Though the single modification strategy have their own merits, a single modification strategy is difficult to simultaneously realize the improvement of structural stability, energy density, and rate performance. However, the synergistic mechanism of multiple modification strategies on the electrochemical performance of cathode materials still needs to be explored. Moreover, to realize the practical application of Mn-based oxide cathodes, further optimization should be carried out at the level of the whole battery, involving the constant optimization of various components, including functional electrolytes, multifunctional separators, and anode materials. Meanwhile, the comprehensive cost and profit should also be taken into account. In addition, the storage mechanism of each cathode material needs to be clarified.

AUTHOR INFORMATION

Corresponding Authors

Shouyi Yuan − *National and Local Joint Engineering Laboratory for Lithium-ion Batteries and Materials Preparation Technology, Key Laboratory of Advanced Battery Materials of Yunnan Province, Faculty of Metallurgical and Energy Engineering Kunming, Kunming University of Science and Technology, Kunming 650093, PR China*; Email: 20210072@kust.edu.cn

Yannan Zhang − *National and Local Joint Engineering Laboratory for Lithium-ion Batteries and Materials Preparation Technology, Key Laboratory of Advanced Battery Materials of Yunnan Province, Faculty of Metallurgical and Energy Engineering Kunming, Kunming University of Science and Technology, Kunming 650093, PR China*; Email: 20200002@kust.edu.cn

Yonggang Wang − *Department of Chemistry, Shanghai Key Laboratory of Catalysis and Innovative Materials, Center of Chemistry for Energy Materials, Shanghai 200433, PR China*; orcid.org/0000-0002-2447-4679; Email: ygwang@fudan.edu.cn

Authors

Bao Zhang − *National and Local Joint Engineering Laboratory for Lithium-ion Batteries and Materials Preparation Technology, Key Laboratory of Advanced Battery Materials of Yunnan Province, Faculty of Metallurgical and Energy Engineering Kunming, Kunming University of Science and Technology, Kunming 650093, PR China*

Peng Dong − *National and Local Joint Engineering Laboratory for Lithium-ion Batteries and Materials Preparation Technology, Key Laboratory of Advanced Battery Materials of Yunnan Province, Faculty of Metallurgical and Energy Engineering Kunming, Kunming University of Science and Technology, Kunming 650093, PR China*

Yingjie Zhang − *National and Local Joint Engineering Laboratory for Lithium-ion Batteries and Materials Preparation Technology, Key Laboratory of Advanced Battery Materials of Yunnan Province, Faculty of Metallurgical and Energy Engineering Kunming, Kunming University of Science and Technology, Kunming 650093, PR China*

Complete contact information is available at: https://pubs.acs.org/10.1021/cbe.3c00120

Notes

The authors declare no competing financial interest.

ACKNOWLEDGMENTS

We acknowledge the funding from the National Natural Science Foundation of China (52164031, 52204312), the Basic Research Plan of Yunnan Province, China (202201AT070160, 202101AU070048, 202101AT070449), the Key Research and Development Program of Yunnan Province, China (202103AA080019), and the Natural Science Key Foundation of Yunnan Province, China (202101BE070001-003), as well as Yunnan Major Scientific and Technological Projects (Grant No. 202202AG050003).

REFERENCES

(1) Creutzig, F.; Agoston, P.; Goldschmidt, J. C.; Luderer, G.; Nemet, G.; Pietzcker, R. C. The underestimated potential of solar energy to mitigate climate change. *Nat. Energy* **2017**, *2* (9), 17140.

(2) Zhang, Y.; Liu, N. Nanostructured Electrode Materials for High-Energy Rechargeable Li, Na and Zn Batteries. *Chem. Mater.* **2017**, *29* (22), 9589−9604.

(3) Chu, S.; Cui, Y.; Liu, N. The path towards sustainable energy. *Nat. Mater.* **2017**, *16* (1), 16−22.

(4) Bin, D.; Wang, F.; Tamirat, A. G.; Suo, L. M.; Wang, Y. G.; Wang, C. S.; Xia, Y. Y. Progress in Aqueous Rechargeable Sodium-Ion Batteries. *Adv. Energy Mater.* **2018**, *8* (17), 1703008.

(5) Kim, H.; Hong, J.; Park, K. Y.; Kim, H.; Kim, S. W.; Kang, K. Aqueous rechargeable Li and Na ion batteries. *Chem. Rev.* **2014**, *114* (23), 11788−827.
(6) Cheng, D. X.; Li, Y. H.; Zhang, J. L.; Tian, M. R.; Wang, B. Y.; He, Z. X.; Dai, L.; Wang, L. Recent advances in electrospun carbon fiber electrode for vanadium redox flow battery: Properties, structures, and perspectives. *Carbon* **2020**, *170*, 527−542.
(7) Zubi, G.; Dufo-Lopez, R.; Carvalho, M.; Pasaoglu, G. The lithium-ion battery: State of the art and future perspectives. *Renewable Sustainable Energy Rev.* **2018**, *89*, 292−308.
(8) Etacheri, V.; Marom, R.; Elazari, R.; Salitra, G.; Aurbach, D. Challenges in the development of advanced Li-ion batteries: a review. *Energy Environ. Sci.* **2011**, *4* (9), 3243−3262.
(9) Saw, L. H.; Ye, Y. H.; Tay, A. A. O. Integration issues of lithium-ion battery into electric vehicles battery pack. *J. Cleaner Prod* **2016**, *113*, 1032−1045.
(10) Posada, J. O. G.; Rennie, A. J. R.; Villar, S. P.; Martins, V. L.; Marinaccio, J.; Barnes, A.; Glover, C. F.; Worsley, D. A.; Hall, P. J. Aqueous batteries as grid scale energy storage solutions. *Renewable Sustainable Energy Rev.* **2017**, *68*, 1174−1182.
(11) Ordoñez, J.; Gago, E. J.; Girard, A. Processes and technologies for the recycling and recovery of spent lithium-ion batteries. *Renewable and Sustainable Energy Reviews* **2016**, *60*, 195−205.
(12) Huang, W. Z.; Zhao, C. Z.; Wu, P.; Yuan, H.; Feng, W. E.; Liu, Z. Y.; Lu, Y.; Sun, S.; Fu, Z. H.; Hu, J. K.; Yang, S. J.; Huang, J. Q.; Zhang, Q. Anode-Free Solid-State Lithium Batteries: A Review. *Adv. Energy Mater.* **2022**, *12* (26), 2201044.
(13) Kobayashi, T.; Ohnishi, T.; Osawa, T.; Pratt, A.; Tear, S.; Shimoda, S.; Baba, H.; Laitinen, M.; Sajavaara, T. In-Operando Lithium-Ion Transport Tracking in an All-Solid-State Battery. *Small* **2022**, *18*, No. e2204455.
(14) Zhang, R.; Shen, X.; Zhang, Y. T.; Zhong, X. L.; Ju, H. T.; Huang, T. X.; Chen, X.; Zhang, J. D.; Huang, J. Q. Dead lithium formation in lithium metal batteries: A phase field model. *J. Energy Chem.* **2022**, *71*, 29−35.
(15) Turcheniuk, K.; Bondarev, D.; Singhal, V.; Yushin, G. Ten years left to redesign lithium-ion batteries. *Nature* **2018**, *559* (7715), 467−470.
(16) Wang, Y. Q.; An, N.; Wen, L.; Wang, L.; Jiang, X. T.; Hou, F.; Yin, Y. X.; Liang, J. Recent progress on the recycling technology of Li-ion batteries. *J. Energy Chem.* **2021**, *55*, 391−419.
(17) Blanc, L. E.; Kundu, D.; Nazar, L. F. Scientific Challenges for the Implementation of Zn-Ion Batteries. *Joule* **2020**, *4* (4), 771−799.
(18) Zuo, S.; Xu, X.; Ji, S.; Wang, Z.; Liu, Z.; Liu, J. Cathodes for Aqueous Zn-Ion Batteries: Materials, Mechanisms, and Kinetics. *Chemistry* **2021**, *27* (3), 830−860.
(19) Zeng, X. H.; Hao, J. N.; Wang, Z. J.; Mao, J. F.; Guo, Z. P. Recent progress and perspectives on aqueous Zn-based rechargeable batteries with mild aqueous electrolytes. *Energy Storage Mater.* **2019**, *20*, 410−437.
(20) Zhang, H.; Liu, X.; Li, H.; Hasa, I.; Passerini, S. Challenges and Strategies for High-Energy Aqueous Electrolyte Rechargeable Batteries. *Angew. Chem. Int. Ed. Engl.* **2021**, *60* (2), 598−616.
(21) Liu, Z.; Huang, Y.; Huang, Y.; Yang, Q.; Li, X.; Huang, Z.; Zhi, C. Voltage issue of aqueous rechargeable metal-ion batteries. *Chem. Soc. Rev.* **2020**, *49* (1), 180−232.
(22) Wang, H. P.; Tan, R.; Yang, Z. X.; Feng, Y. Z.; Duan, X. C.; Ma, J. M. Stabilization Perspective on Metal Anodes for Aqueous Batteries. *Adv. Energy Mater.* **2021**, *11* (2), 2000962.
(23) Demir-Cakan, R.; Palacin, M. R.; Croguennec, L. Rechargeable aqueous electrolyte batteries: from univalent to multivalent cation chemistry. *J. Mater. Chem. A* **2019**, *7* (36), 20519−20539.
(24) Selvakumaran, D.; Pan, A. Q.; Liang, S. Q.; Cao, G. Z. A review on recent developments and challenges of cathode materials for rechargeable aqueous Zn-ion batteries. *J. Mater. Chem. A* **2019**, *7* (31), 18209−18236.
(25) Chao, D.; Zhou, W.; Xie, F.; Ye, C.; Li, H.; Jaroniec, M.; Qiao, S. Z. Roadmap for advanced aqueous batteries: From design of materials to applications. *Sci. Adv.* **2020**, *6* (21), No. eaba4098.
(26) Jia, X.; Liu, C.; Neale, Z. G.; Yang, J.; Cao, G. Active Materials for Aqueous Zinc Ion Batteries: Synthesis, Crystal Structure, Morphology, and Electrochemistry. *Chem. Rev.* **2020**, *120* (15), 7795−7866.
(27) Guo, Y.; Zhang, Y.; Lu, H. Manganese-based materials as cathode for rechargeable aqueous zinc-ion batteries. *Battery Energy* **2022**, *1* (2), 20210014.
(28) Piccolino, M. The bicentennial of the Voltaic battery (1800-2000): the artificial electric organ. *Trends Neurosci.* **2000**, *23* (4), 147−151.
(29) Mainar, A. R.; Colmenares, L. C.; Blazquez, J. A.; Urdampilleta, I. A brief overview of secondary zinc anode development: The key of improving zinc-based energy storage systems. *Int. J. Energy Res.* **2018**, *42* (3), 903−918.
(30) Zhang, N.; Cheng, F.; Liu, J.; Wang, L.; Long, X.; Liu, X.; Li, F.; Chen, J. Rechargeable aqueous zinc-manganese dioxide batteries with high energy and power densities. *Nat. Commun.* **2017**, *8* (1), 405.
(31) Shoji, T.; Hishinuma, M.; Yamamoto, T. Zinc-manganese dioxide galvanic cell using zinc sulphate as electrolyte. Rechargeability of the cell. *J. Appl. Electrochem.* **1988**, *18* (4), 521−526.
(32) Xu, C. J.; Li, B. H.; Du, H. D.; Kang, F. Y. Energetic Zinc Ion Chemistry: The Rechargeable Zinc Ion Battery. *Angew. Chem.-Int. Ed.* **2012**, *51* (4), 933−935.
(33) Li, H. F.; Ma, L. T.; Han, C. P.; Wang, Z. F.; Liu, Z. X.; Tang, Z. J.; Zhi, C. Y. Advanced rechargeable zinc-based batteries: Recent progress and future perspectives. *Nano Energy* **2019**, *62*, 550−587.
(34) Xu, D. W.; Li, B. H.; Wei, C. G.; He, Y. B.; Du, H. D.; Chu, X. D.; Qin, X. Y.; Yang, Q. H.; Kang, F. Y. Preparation and Characterization of MnO_2/acid-treated CNT Nanocomposites for Energy Storage with Zinc Ions. *Electrochim. Acta* **2014**, *133*, 254−261.
(35) Tafur, J. P.; Abad, J.; Román, E.; Fernández Romero, A. J. Charge storage mechanism of MnO_2 cathodes in Zn/MnO_2 batteries using ionic liquid-based gel polymer electrolytes. *Electrochem. Commun.* **2015**, *60*, 190−194.
(36) Wei, C. G.; Xu, C. J.; Li, B. H.; Du, H. D.; Kang, F. Y. Preparation and characterization of manganese dioxides with nano-sized tunnel structures for zinc ion storage. *J. Phys. Chem. Solids* **2012**, *73* (12), 1487−1491.
(37) Sambandam, B.; Soundharrajan, V.; Kim, S.; Alfaruqi, M. H.; Jo, J.; Kim, S.; Mathew, V.; Sun, Y. K.; Kim, J. Aqueous rechargeable Zn-ion batteries: an imperishable and high-energy $Zn_2V_2O_7$ nanowire cathode through intercalation regulation. *J. Mater. Chem. A* **2018**, *6* (9), 3850−3856.
(38) Chen, L.; Yang, Z.; Cui, F.; Meng, J.; Zeng, X. Enhanced rate and cycling performances of hollow V_2O_5 nanospheres for aqueous zinc ion battery cathode. *Appl. Surf. Sci.* **2020**, *507*, 145137.
(39) He, P.; Quan, Y.; Xu, X.; Yan, M.; Yang, W.; An, Q.; He, L.; Mai, L. High-Performance Aqueous Zinc-Ion Battery Based on Layered $H_2V_3O_8$ Nanowire Cathode. *Small* **2017**, *13* (47), 1702551.
(40) Hu, P.; Yan, M.; Zhu, T.; Wang, X.; Wei, X.; Li, J.; Zhou, L.; Li, Z.; Chen, L.; Mai, L. Zn/V_2O_5 Aqueous Hybrid-Ion Battery with High Voltage Platform and Long Cycle Life. *ACS Appl. Mater. Interfaces* **2017**, *9* (49), 42717−42722.
(41) Wessells, C. D.; Huggins, R. A.; Cui, Y. Copper hexacyanoferrate battery electrodes with long cycle life and high power. *Nat. Commun.* **2011**, *2* (1), 550.
(42) Lee, H. W.; Wang, R. Y.; Pasta, M.; Woo Lee, S.; Liu, N.; Cui, Y. Manganese hexacyanomanganate open framework as a high-capacity positive electrode material for sodium-ion batteries. *Nat. Commun.* **2014**, *5* (1), 5280.
(43) You, Y.; Wu, X. L.; Yin, Y. X.; Guo, Y. G. High-quality Prussian blue crystals as superior cathode materials for room-temperature sodium-ion batteries. *Energy Environ. Sci.* **2014**, *7* (5), 1643−1647.
(44) Glatz, H.; Lizundia, E.; Pacifico, F.; Kundu, D. An Organic Cathode Based Dual-Ion Aqueous Zinc Battery Enabled by a Cellulose Membrane. *ACS Appl. Energy Mater.* **2019**, *2* (2), 1288.
(45) Dawut, G.; Lu, Y.; Miao, L. C.; Chen, J. High-performance rechargeable aqueous Zn-ion batteries with a poly(benzoquinonyl sulfide) cathode. *Inorg. Chem. Front* **2018**, *5* (6), 1391−1396.

https://doi.org/10.1021/cbe.3c00120
Chem Bio Eng. 2024, 1, 113−132

(46) Schon, T. B.; Mcallister, B. T.; Li, P. F.; Seferos, D. S. The rise of organic electrode materials for energy storage. *Chem. Soc. Rev.* **2016**, *45*, 6345.
(47) Shi, Y.; Chen, Y.; Shi, L.; Wang, K.; Wang, B.; Li, L.; Ma, Y.; Li, Y.; Sun, Z.; Ali, W.; Ding, S. An Overview and Future Perspectives of Rechargeable Zinc Batteries. *Small* **2020**, *16* (23), No. e2000730.
(48) Mathew, V.; Sambandam, B.; Kim, S.; Kim, S.; Park, S.; Lee, S.; Alfaruqi, M. H.; Soundharrajan, V.; Islam, S.; Putro, D. Y.; Hwang, J. Y.; Sun, Y. K.; Kim, J. Manganese and Vanadium Oxide Cathodes for Aqueous Rechargeable Zinc-Ion Batteries: A Focused View on Performance, Mechanism, and Developments. *Acs Energy Letters* **2020**, *5* (7), 2376−2400.
(49) Post, J. E. Manganese oxide minerals: crystal structures and economic and environmental significance. *Proc. Natl. Acad. Sci. U. S. A.* **1999**, *96* (7), 3447−54.
(50) Li, H. X.; Zhang, W.; Sun, K. N.; Guo, J.; Yuan, K.; Fu, J. J.; Zhang, T.; Zhang, X. K.; Long, H. W.; Zhang, Z. A.; Lai, Y. Q.; Sun, H. Y. Manganese-Based Materials for Rechargeable Batteries beyond Lithium-Ion. *Adv. Energy Mater.* **2021**, *11* (25), 2100867.
(51) Yuan, Y. F.; Liu, C.; Byles, B. W.; Yao, W. T.; Song, B.; Cheng, M.; Huang, Z. N.; Amine, K.; Pomerantseva, E.; Shahbazian-Yassar, R.; Lu, J. Ordering Heterogeneity of [MnO_6] Octahedra in Tunnel-Structured MnO_2 and Its Influence on Ion Storage. *Joule* **2019**, *3* (2), 471−484.
(52) Han, M. M.; Qin, L. P.; Liu, Z. X.; Zhang, L. X.; Li, X. K.; Lu, B. A.; Huang, J. W.; Liang, S. Q.; Zhou, J. Reaction mechanisms and optimization strategies of manganese-based materials for aqueous zinc batteries. *Mater. Today Energy* **2021**, *20*, 100626.
(53) Zhang, Z.; Li, W.; Shen, Y.; Wang, R.; Li, H.; Zhou, M.; Wang, W.; Wang, K.; Jiang, K. Issues and opportunities of manganese-based materials for enhanced Zn-ion storage performances. *J. Energy Storage* **2022**, *45*, 103729.
(54) Alfaruqi, M. H.; Gim, J.; Kim, S.; Song, J.; Jo, J.; Kim, S.; Mathew, V.; Kim, J. Enhanced reversible divalent zinc storage in a structurally stable α-MnO_2 nanorod electrode. *J. Power Sources* **2015**, *288*, 320−327.
(55) Islam, S.; Alfaruqi, M. H.; Song, J.; Kim, S.; Pham, D. T.; Jo, J.; Kim, S.; Mathew, V.; Baboo, J. P.; Xiu, Z.; Kim, J. Carbon-coated manganese dioxide nanoparticles and their enhanced electrochemical properties for zinc-ion battery applications. *J. Energy Chem.* **2017**, *26* (4), 815−819.
(56) Islam, S.; Alfaruqi, M. H.; Mathew, V.; Song, J.; Kim, S.; Kim, S.; Jo, J.; Baboo, J. P.; Pham, D. T.; Putro, D. Y.; Sun, Y.-K.; Kim, J. Facile synthesis and the exploration of the zinc storage mechanism of β-MnO_2 nanorods with exposed (101) planes as a novel cathode material for high performance eco-friendly zinc-ion batteries. *J. Mater. Chem. A* **2017**, *5* (44), 23299−23309.
(57) Qiu, N.; Chen, H.; Yang, Z. M.; Sun, S.; Wang, Y. Low-cost birnessite as a promising cathode for high-performance aqueous rechargeable batteries. *Electrochim. Acta* **2018**, *272*, 154−160.
(58) Alfaruqi, M. H.; Islam, S.; Putro, D. Y.; Mathew, V.; Kim, S.; Jo, J.; Kim, S.; Sun, Y. K.; Kim, K.; Kim, J. Structural transformation and electrochemical study of layered MnO_2 in rechargeable aqueous zinc-ion battery. *Electrochim. Acta* **2018**, *276*, 1−11.
(59) Xu, C. J.; Chen, Y. Y.; Shi, S.; Li, J.; Kang, F. Y.; Su, D. S. Secondary batteries with multivalent ions for energy storage. *Sci. Rep* **2015**, *5* (1), 14120.
(60) Ming, J.; Guo, J.; Xia, C.; Wang, W. X.; Alshareef, H. N. Zinc-ion batteries: Materials, mechanisms, and applications. *Mat Sci. Eng. R* **2019**, *135*, 58−84.
(61) Lee, B.; Lee, H. R.; Kim, H.; Chung, K. Y.; Cho, B. W.; Oh, S. H. Elucidating the intercalation mechanism of zinc ions into alpha-MnO_2 for rechargeable zinc batteries. *Chem. Commun. (Camb.)* **2015**, *51* (45), 9265−8.
(62) Wang, Y.; et al. Facile synthesis and the exploration of the zinc storage mechanism of β-MnO_2 nanorods with exposed (101) planes as a novel cathode material for high performance eco-friendly zinc-ion batteries. *J. Mater. Chem. A* **2017**, *5*, 18674.
(63) Alfaruqi, M. H.; Mathew, V.; Gim, J.; Kim, S.; Kim, J. Electrochemically Induced Structural Transformation in a γ-MnO_2 Cathode of a High Capacity Zinc-Ion Battery System. *Chem. Mater.* **2015**, *27* (10), 3609.
(64) Wang, D.; Wang, L.; Liang, G.; Li, H.; Zhi, C. A Superior δ-MnO_2 Cathode and a Self-Healing Zn-δ-MnO_2 Battery. *ACS Nano* **2019**, *13* (9), 10643.
(65) Yuan, C.; Zhang, Y.; Pan, Y.; Liu, X.; Wang, G.; Cao, D. Investigation of the intercalation of polyvalent cations (Mg^{2+}, Zn^{2+}) into λ-MnO_2 for rechargeable aqueous battery. *Electrochim. Acta* **2014**, *116*, 404−412.
(66) Zhang, Y.; Liu, Y.; Liu, Z.; Wu, X.; Wen, Y.; Chen, H.; Ni, X.; Liu, G.; Huang, J.; Peng, S. MnO_2 cathode materials with the improved stability via nitrogen doping for aqueous zinc-ion batteries. *J. Energy Chem.* **2022**, *64*, 23−32.
(67) Zhang, Z. N.; Shang, H. J.; Zhang, X. L.; Liu, C.; Li, S.; Wen, Z. S.; Ji, S. J.; Sun, J. C. Enhancing the Electrochemical Performances by Wet Ball Milling to Introduce Structural Water into an Electrolytic MnO/Graphite Nanocomposite Cathode for Zinc-Ion Batteries. *ACS Appl. Energy Mater.* **2021**, *4* (5), 5113−5122.
(68) Cockayne, E.; Levin, I.; Wu, H.; Llobet, A. Magnetic structure of bixbyite α-Mn_2O_3: A combined DFT+U and neutron diffraction study. *Phys. Rev.* **2013**, *87* (18), 184413.
(69) Jiang, B. Z.; Xu, C. J.; Wu, C. L.; Dong, L. B.; Li, J.; Kang, F. Y. Manganese Sesquioxide as Cathode Material for Multivalent Zinc Ion Battery with High Capacity and Long Cycle Life. *Electrochim. Acta* **2017**, *229*, 422−428.
(70) Hao, J. W.; Mou, J.; Zhang, J. W.; Dong, L. B.; Liu, W. B.; Xu, C. J.; Kang, F. Y. Electrochemically induced spinel-layered phase transition of Mn_3O_4 in high performance neutral aqueous rechargeable zinc battery. *Electrochim. Acta* **2018**, *259*, 170−178.
(71) Wang, J. J.; Wang, J. G.; Liu, H. Y.; You, Z. Y.; Wei, C. G.; Kang, F. Y. Electrochemical activation of commercial MnO microsized particles for high-performance aqueous zinc-ion batteries. *J. Power Sources* **2019**, *438*, 226951.
(72) Yu, P.; Zhou, J.; Zheng, M.; Li, M.; Hu, H.; Xiao, Y.; Liu, Y.; Liang, Y. Boosting Zinc Ion Energy Storage Capability of Inert MnO Cathode by Defect Engineering. *J. Colloid Interface Sci.* **2021**, *594*, 540.
(73) Yao, H.; Yu, H.; Zheng, Y.; Li, N. W.; Li, S.; Luan, D.; Lou, X. W.; Yu, L. Pre-intercalation of Ammonium Ions in Layered δ-MnO_2 Nanosheets for High-Performance Aqueous Zinc-Ion Batteries. *Angew. Chem., Int. Ed* **2023**, *62* (51), e202315257.
(74) Zhao, Y.; Zhang, S.; Zhang, Y.; Liang, J.; Ren, L.; Fan, H. J.; Liu, W.; Sun, X. Vacancy-rich Al-doped MnO_2 cathodes break the trade-off between kinetics and stability for high-performance aqueous Zn-ion batteries. *Energy Environ. Sci.* **2024**, *17*, 1279.
(75) Zhang, J.; Li, W.; Wang, J.; Pu, X.; Zhang, G.; Wang, S.; Wang, N.; Li, X. Engineering p-Band Center of Oxygen Boosting H^+ Intercalation in δ-MnO_2 for Aqueous Zinc Ion Batteries. *Angew. Chem., Int. Ed* **2023**, *62* (8), e202215654.
(76) Wu, B.; Zhang, G.; Yan, M.; Xiong, T.; He, P.; He, L.; Xu, X.; Mai, L. Graphene Scroll-Coated α-MnO_2 Nanowires as High-Performance Cathode Materials for Aqueous Zn-Ion Battery. *Small* **2018**, *14* (13), No. e1703850.
(77) Han, R.; Pan, Y.; Du, C.; Xiang, Y.; Wang, Y.; Zhu, H.; Yin, C. Eu doping β-MnO_2 as cathode materials for high specific capacity aqueous zinc ion batteries. *J. Energy Storage* **2024**, *80*, 110250.
(78) Xiao, X.; Zhang, L.; Xin, W.; Yang, M.; Geng, Y.; Niu, M.; Zhang, H.; Zhu, Z. Self-Assembled Layer of Organic Phosphonic Acid Enables Highly Stable MnO_2 Cathode for Aqueous Znic Batteries. *Small* **2024**, DOI: 10.1002/smll.202309271.
(79) Zeng, X.; Liu, J.; Mao, J.; Hao, J.; Wang, Z.; Zhou, S.; Ling, C. D.; Guo, Z. Toward a Reversible Mn^{4+}/Mn^{2+} Redox Reaction and Dendrite-Free Zn Anode in Near-Neutral Aqueous Zn/MnO_2 Batteries via Salt Anion Chemistry. *Adv. Energy Mater.* **2020**, *10* (32), 1904163.
(80) Huang, C. F.; Wu, C.; Zhang, Z. L.; Xie, Y. Y.; Li, Y.; Yang, C. H.; Wang, H. Crystalline and amorphous MnO cathodes with open

framework enable high-performance aqueous zinc-ion batteries. *Front. Mater. Sci.* **2021**, *15* (2), 202−215.
(81) Wang, D. H.; Wang, L. F.; Liang, G. J.; Li, H. F.; Liu, Z. X.; Tang, Z. J.; Liang, J. B.; Zhi, C. Y. A Superior δ-MnO Cathode and a Self-Healing Zn-δ-MnO Battery. *ACS Nano* **2019**, *13* (9), 10643−10652.
(82) Lee, B.; Seo, H. R.; Lee, H. R.; Yoon, C. S.; Kim, J. H.; Chung, K. Y.; Cho, B. W.; Oh, S. H. Critical Role of pH Evolution of Electrolyte in the Reaction Mechanism for Rechargeable Zinc Batteries. *ChemSusChem* **2016**, *9* (20), 2948−2956.
(83) Zhu, C. Y.; Fang, G. Z.; Liang, S. Q.; Chen, Z. X.; Wang, Z. Q.; Ma, J. Y.; Wang, H.; Tang, B. Y.; Zheng, X. S.; Zhou, J. Electrochemically induced cationic defect in MnO intercalation cathode for aqueous zinc-ion battery. *Energy Storage Mater.* **2020**, *24*, 394−401.
(84) Wang, J. J.; Wang, J. G.; Liu, H. Y.; You, Z. Y.; Wei, C. G.; Kang, F. Y. Electrochemical activation of commercial MnO microsized particles for high-performance aqueous zinc-ion batteries. *J. Power Sources* **2019**, *438*, 226951.
(85) Huang, J.; Zeng, J.; Zhu, K.; Zhang, R.; Liu, J. High-Performance Aqueous Zinc-Manganese Battery with Reversible Mn^{2+}/Mn^{4+} Double Redox Achieved by Carbon Coated MnO_x Nanoparticles. *Nano-Micro Letters* **2020**, *12* (1), 110.
(86) Fu, Y.; Wei, Q.; Zhang, G.; Wang, X.; Zhang, J.; Hu, Y.; Wang, D.; Zuin, L.; Zhou, T.; Wu, Y.; Sun, S. High-Performance Reversible Aqueous Zn-Ion Battery Based on Porous MnO_x Nanorods Coated by MOF-Derived N-Doped Carbon. *Adv. Energy Mater.* **2018**, *8* (26), 1801445.
(87) Wang, L. L.; Cao, X.; Xu, L. H.; Chen, J. T.; Zheng, J. R. Transformed Akhtenskite MnO from MnO as Cathode for a Rechargeable Aqueous Zinc Ion Battery. *Acs Sustainable Chemistry & Engineering* **2018**, *6* (12), 16055−16063.
(88) Hao, J. W.; Mou, J.; Zhang, J. W.; Dong, L. B.; Liu, W. B.; Xu, C. J.; Kang, F. Y. Electrochemically induced spinel-layered phase transition of MnO in high performance neutral aqueous rechargeable zinc battery. *Electrochim. Acta* **2018**, *259*, 170−178.
(89) Tan, Q.; Li, X.; Zhang, B.; Chen, X.; Tian, Y.; Wan, H.; Zhang, L.; Miao, L.; Wang, C.; Gan, Y.; Jiang, J.; Wang, Y.; Wang, H. Valence Engineering via In Situ Carbon Reduction on Octahedron Sites Mn_3O_4 for Ultra-Long Cycle Life Aqueous Zn-Ion Battery. *Adv. Energy Mater.* **2020**, *10* (38), 2001050.
(90) Yuan, Y.; Sharpe, R.; He, K.; Li, C.; Saray, M. T.; Liu, T.; Yao, W.; Cheng, M.; Jin, H.; Wang, S.; Amine, K.; Shahbazian-Yassar, R.; Islam, M. S.; Lu, J. Understanding intercalation chemistry for sustainable aqueous zinc-manganese dioxide batteries. *Nature Sustainability* **2022**, *5* (10), 890−898.
(91) Sambandam, B.; Mathew, V.; Kim, S.; Lee, S.; Kim, S.; Hwang, J. Y.; Fan, H. J.; Kim, J. An analysis of the electrochemical mechanism of manganese oxides in aqueous zinc batteries. *Chem.* **2022**, *8* (4), 924−946.
(92) Liu, N.; Li, B.; He, Z. X.; Dai, L.; Wang, H. Y.; Wang, L. Recent advances and perspectives on vanadium- and manganese-based cathode materials for aqueous zinc ion batteries. *J. Energy Chem.* **2021**, *59*, 134−159.
(93) Guo, X.; Fang, G.; Zhang, W.; Zhou, J.; Shan, L.; Wang, L.; Wang, C.; Lin, T.; Tang, Y.; Liang, S. Mechanistic Insights of Zn^{2+} Storage in Sodium Vanadates. *Adv. Energy Mater.* **2018**, *8* (27), 1801819.
(94) Alfaruqi, M. H.; Mathew, V.; Gim, J.; Kim, S.; Song, J.; Baboo, J. P.; Choi, S. H.; Kim, J. Electrochemically Induced Structural Transformation in a γ-MnO2Cathode of a High Capacity Zinc-Ion Battery System. *Chem. Mater.* **2015**, *27* (10), 3609−3620.
(95) Pan, H. L.; Shao, Y. Y.; Yan, P. F.; Cheng, Y. W.; Han, K. S.; Nie, Z. M.; Wang, C. M.; Yang, J. H.; Li, X. L.; Bhattacharya, P.; Mueller, K. T.; Liu, J. Reversible aqueous zinc/manganese oxide energy storage from conversion reactions. *Nat. Energy* **2016**, *1* (5), 16039.
(96) Liu, W.; Zhang, X.; Huang, Y.; Jiang, B.; Chang, Z.; Xu, C.; Kang, F. β-MnO_2 with proton conversion mechanism in rechargeable zinc ion battery. *J. Energy Chem.* **2021**, *56*, 365−373.
(97) Zhu, C.; Fang, G.; Zhou, J.; Guo, J.; Wang, Z.; Wang, C.; Li, J.; Tang, Y.; Liang, S. Binder-free stainless steel@Mn_3O_4 nanoflower composite: a high-activity aqueous zinc-ion battery cathode with high-capacity and long-cycle-life. *J. Mater. Chem. A* **2018**, *6* (20), 9677−9683.
(98) Yang, H.; Zhou, W.; Chen, D.; Liu, J.; Yuan, Z.; Lu, M.; Shen, L.; Shulga, V.; Han, W.; Chao, D. The origin of capacity fluctuation and rescue of dead Mn-based Zn-ion batteries: a Mn-based competitive capacity evolution protocol. *Energy Environ. Sci.* **2022**, *15* (3), 1106−1118.
(99) Zhao, Q.; Chen, X.; Wang, Z.; Yang, L.; Qin, R.; Yang, J.; Song, Y.; Ding, S.; Weng, M.; Huang, W.; Liu, J.; Zhao, W.; Qian, G.; Yang, K.; Cui, Y.; Chen, H.; Pan, F. Unravelling H^+/Zn^{2+} Synergistic Intercalation in a Novel Phase of Manganese Oxide for High-Performance Aqueous Rechargeable Battery. *Small* **2019**, *15* (47), No. e1904545.
(100) Sun, W.; Wang, F.; Hou, S.; Yang, C.; Fan, X.; Ma, Z.; Gao, T.; Han, F.; Hu, R.; Zhu, M.; Wang, C. Zn/MnO_2 Battery Chemistry With H^+ and Zn^{2+} Coinsertion. *J. Am. Chem. Soc.* **2017**, *139* (29), 9775−9778.
(101) Gao, X.; Wu, H.; Li, W.; Tian, Y.; Zhang, Y.; Wu, H.; Yang, L.; Zou, G.; Hou, H.; Ji, X. H^+-Insertion Boosted alpha-MnO_2 for an Aqueous Zn-Ion Battery. *Small* **2020**, *16* (5), No. e1905842.
(102) Li, Y.; Wang, S.; Salvador, J. R.; Wu, J.; Liu, B.; Yang, W.; Yang, J.; Zhang, W.; Liu, J.; Yang, J. Reaction Mechanisms for Long-Life Rechargeable Zn/MnO_2 Batteries. *Chem. Mater.* **2019**, *31* (6), 2036−2047.
(103) Fenta, F. W.; Olbasa, B. W.; Tsai, M.-C.; Weret, M. A.; Zegeye, T. A.; Huang, C.-J.; Huang, W.-H.; Zeleke, T. S.; Sahalie, N. A.; Pao, C.-W.; Wu, S.-h.; Su, W.-N.; Dai, H.; Hwang, B. J. Electrochemical transformation reaction of Cu-MnO in aqueous rechargeable zinc-ion batteries for high performance and long cycle life. *J. Mater. Chem. A* **2020**, *8* (34), 17595−17607.
(104) Wang, J. J.; Wang, J. G.; Liu, H. Y.; You, Z. Y.; Wei, C. G.; Kang, F. Y. Electrochemical activation of commercial MnO microsized particles for high-performance aqueous zinc-ion batteries. *J. Power Sources* **2019**, *438*, 226951.
(105) Liang, G. J.; Mo, F. N.; Li, H. F.; Tang, Z. J.; Liu, Z. X.; Wang, D. H.; Yang, Q.; Ma, L. T.; Zhi, C. Y. A Universal Principle to Design Reversible Aqueous Batteries Based on Deposition-Dissolution Mechanism. *Adv. Energy Mater.* **2019**, *9* (32), 1901838.
(106) Soundharrajan, V.; Sambandam, B.; Kim, S.; Islam, S.; Jo, J.; Kim, S.; Mathew, V.; Sun, Y. K.; Kim, J. The dominant role of Mn^{2+} additive on the electrochemical reaction in $ZnMn_2O_4$ cathode for aqueous zinc-ion batteries. *Energy Storage Mater.* **2020**, *28*, 407−417.
(107) Guo, X.; Zhou, J.; Bai, C. L.; Li, X. K.; Fang, G. Z.; Liang, S. Q. Zn/MnO_2 battery chemistry with dissolution-deposition mechanism. *Mater. Today Energy* **2020**, *16*, 100396.
(108) Cui, S.; Zhang, D.; Gan, Y. Traditional Electrochemical Zn^{2+} Intercalation/Extraction Mechanism Revisited: Unveiling Ion-Exchange Mediated Irreversible Zn^{2+} Intercalation for the δ-MnO_2 Cathode in Aqueous Zn Ion Batteries. *Adv. Energy Mater.* **2024**, DOI: 10.1002/aenm.202302655.
(109) Ye, X. L.; Han, D. L.; Jiang, G. Y.; Cui, C. J.; Guo, Y.; Wang, Y. G.; Zhang, Z. C.; Weng, Z.; Yang, Q. H. Unraveling the deposition/dissolution chemistry of MnO for high-energy aqueous batteries. *Energy Environ. Sci.* **2023**, *16* (3), 1016−1023.
(110) Liu, Y.; Ma, Y.; Yang, W.; Bao, S.; Chen, H.; Xu, M. Spontaneously dissolved MnO: A better cathode material for rechargeable aqueous zinc-manganese batteries. *Chem. Eng. J.* **2023**, *473*, 145490.
(111) Wu, T.-H.; Lin, Y.-Q.; Althouse, Z. D.; Liu, N. Dissolution-Redeposition Mechanism of the MnO_2 Cathode in Aqueous Zinc-Ion Batteries. *ACS Appl. Energy Mater.* **2021**, *4* (11), 12267−12274.

(112) Ruan, P.; Liang, S.; Lu, B.; Fan, H. J.; Zhou, J. Design Strategies for High-Energy-Density Aqueous Zinc Batteries. *Angew. Chem., Int. Ed.* **2022**, *61* (17), e202200598.
(113) Zhang, A. Q.; Zhao, R.; Wang, Y. H.; Yang, J. J.; Wu, C.; Bai, Y. Regulating the electronic structure of manganese-based materials to optimize the performance of zinc-ion batteries. *Energy Environ. Sci.* **2023**, *16* (8), 3240−3301.
(114) Li, Q.; Zhao, Y. J.; Wang, Y. Y.; Khasraw, A. K.; Zhao, Y.; Sun, X. M. Rational Design of Nanostructured MnO Cathode for High-performance Aqueous Zinc Ion Batteries. *Chem. Res. Chin. Univ.* **2023**, *39* (4), 599−611.
(115) Nam, K. W.; Kim, H.; Choi, J. H.; Choi, J. W. Crystal water for high performance layered manganese oxide cathodes in aqueous rechargeable zinc batteries. *Energy Environ. Sci.* **2019**, *12* (6), 1999−2009.
(116) Chen, C.; Shi, M.; Zhao, Y.; Yang, C.; Zhao, L.; Yan, C. Al-Intercalated MnO_2 cathode with reversible phase transition for aqueous Zn-Ion batteries. *Chem. Eng. J.* **2021**, *422*, 130375.
(117) Peng, H.; Fan, H.; Yang, C.; Tian, Y.; Wang, C.; Sui, J. Ultrathin delta-MnO2 nanoflakes with Na^+ intercalation as a high-capacity cathode for aqueous zinc-ion batteries. *RSC Adv.* **2020**, *10* (30), 17702−17712.
(118) Huang, J.; Wang, Z.; Hou, M.; Dong, X.; Liu, Y.; Wang, Y.; Xia, Y. Polyaniline-intercalated manganese dioxide nanolayers as a high-performance cathode material for an aqueous zinc-ion battery. *Nat. Commun.* **2018**, *9* (1), 2906.
(119) Jiang, W.; Xu, X.; Liu, Y.; Tan, L.; Zhou, F.; Xu, Z.; Hu, R. Facile plasma treated β-MnO_2@C hybrids for durable cycling cathodes in aqueous Zn-ion batteries. *J. Alloys Compd.* **2020**, *827*, 154273.
(120) Gao, Q.-L.; Li, D.-S.; Liu, X.-M.; Wang, Y.-F.; Liu, W.-L.; Ren, M.-M.; Kong, F.-G.; Wang, S.-J.; Zhou, R.-C. Biomass-derived mesoporous carbons materials coated by α-Mn_3O_4 with ultrafast zinc-ion diffusion ability as cathode for aqueous zinc ion batteries. *Electrochim. Acta* **2020**, *335*, 135642.
(121) Guo, X. T.; Li, J. M.; Jin, X.; Han, Y. H.; Lin, Y.; Lei, Z. W.; Wang, S. Y.; Qin, L. J.; Jiao, S. H.; Cao, R. G. A Hollow-Structured Manganese Oxide Cathode for Stable Zn-MnO_2 Batteries. *Nanomaterials* **2018**, *8* (5), 301.
(122) Liu, D.-S.; Mai, Y.; Chen, S.; Liu, S.; Ang, E. H.; Ye, M.; Yang, Y.; Zhang, Y.; Geng, H.; Li, C. C. A 1D-3D interconnected δ-MnO_2 nanowires network as high-performance and high energy efficiency cathode material for aqueous zinc-ion batteries. *Electrochim. Acta* **2021**, *370*, 137740.
(123) Long, J.; Yang, Z.; Yang, F.; Cuan, J.; Wu, J. Electrospun core-shell Mn_3O_4/carbon fibers as high-performance cathode materials for aqueous zinc-ion batteries. *Electrochim. Acta* **2020**, *344*, 136155.
(124) Feng, D. Y.; Gao, T. N.; Zhang, L.; Guo, B. K.; Song, S. Y.; Qiao, Z. A.; Dai, S. Boosting High-Rate Zinc-Storage Performance by the Rational Design of Mn_2O_3 Nanoporous Architecture Cathode. *Nano-Micro Letters* **2020**, *12* (1), 14.
(125) Xiong, T.; Yu, Z. G.; Wu, H. J.; Du, Y. H.; Xie, Q. D.; Chen, J. S.; Zhang, Y. W.; Pennycook, S. J.; Lee, W. S. V.; Xue, J. M. Defect Engineering of Oxygen-Deficient Manganese Oxide to Achieve High-Performing Aqueous Zinc Ion Battery. *Adv. Energy Mater.* **2019**, *9* (14), 1803815.
(126) Fang, G. Z.; Zhu, C. Y.; Chen, M. H.; Zhou, J.; Tang, B. Y.; Cao, X. X.; Zheng, X. S.; Pan, A. Q.; Liang, S. Q. Suppressing Manganese Dissolution in Potassium Manganate with Rich Oxygen Defects Engaged High-Energy-Density and Durable Aqueous Zinc-Ion Battery. *Adv. Funct. Mater.* **2019**, *29* (15), 1808375.
(127) Tan, Q. Y.; Li, X. T.; Zhang, B.; Chen, X.; Tian, Y. W.; Wan, H. Z.; Zhang, L. S.; Miao, L.; Wang, C.; Gan, Y.; Jiang, J. J.; Wang, Y.; Wang, H. Valence Engineering via In Situ Carbon Reduction on Octahedron Sites Mn_3O_4 for Ultra-Long Cycle Life Aqueous Zn-Ion Battery. *Adv. Energy Mater.* **2020**, *10* (38), 2001050.
(128) Liu, N.; Wu, X.; Yin, Y.; Chen, A.; Zhao, C.; Guo, Z.; Fan, L.; Zhang, N. Constructing the Efficient Ion Diffusion Pathway by Introducing Oxygen Defects in Mn_2O_3 for High-Performance Aqueous Zinc-Ion Batteries. *ACS Appl. Mater. Interfaces* **2020**, *12* (25), 28199−28205.
(129) Huang, A.; Zhou, W.; Wang, A.; Chen, M.; Tian, Q.; Chen, J. Molten salt synthesis of α-MnO_2/Mn_2O_3 nanocomposite as a high-performance cathode material for aqueous zinc-ion batteries. *J. Energy Chem.* **2021**, *54*, 475−481.
(130) Gou, L.; Mou, K. L.; Fan, X. Y.; Zhao, M. J.; Wang, Y.; Xue, D.; Li, D. L. Mn_2O_3/Al_2O_3 cathode material derived from a metal-organic framework with enhanced cycling performance for aqueous zinc-ion batteries. *Dalton Trans.* **2020**, *49* (3), 711−718.
(131) Tang, F.; Gao, J. Y.; Ruan, Q. Y.; Wu, X. W.; Wu, X. S.; Zhang, T.; Liu, Z. X.; Xiang, Y. H.; He, Z. Q.; Wu, X. M. Graphene-Wrapped MnO/C Composites by MOFs-Derived as Cathode Material for Aqueous Zinc ion Batteries. *Electrochim. Acta* **2020**, *353*, 136570.
(132) Liu, Y.; Chi, X.; Han, Q.; Du, Y.; Huang, J.; Liu, Y.; Yang, J. α-MnO_2 nanofibers/carbon nanotubes hierarchically assembled microspheres: Approaching practical applications of high-performance aqueous Zn-ion batteries. *J. Power Sources* **2019**, *443*, 227244.
(133) Li, D. S.; Gao, Q. L.; Zhang, H.; Wang, Y. F.; Liu, W. L.; Ren, M. M.; Kong, F. G.; Wang, S. J.; Chang, J. MnO_2 particles grown on the surface of N-doped hollow porous carbon nanospheres for aqueous rechargeable zinc ion batteries. *Appl. Surf. Sci.* **2020**, *510*, 145458.
(134) Lei, J.; Yao, Y.; Wang, Z.; Lu, Y.-C. Towards high-areal-capacity aqueous zinc-manganese batteries: promoting MnO_2 dissolution by redox mediators. *Energy Environ. Sci.* **2021**, *14* (8), 4418−4426.
(135) Xie, C. X.; Li, T. Y.; Deng, C. Z.; Song, Y.; Zhang, H. M.; Li, X. F. A highly reversible neutral zinc/manganese battery for stationary energy storage. *Energy Environ. Sci.* **2020**, *13* (1), 135−143.
(136) Geng, Y. F.; Pan, L.; Peng, Z. Y.; Sun, Z. F.; Lin, H. C.; Mao, C. W.; Wang, L.; Dai, L.; Liu, H. D.; Pan, K. M.; Wu, X. W.; Zhang, Q. B.; He, Z. X. Electrolyte additive engineering for aqueous Zn ion batteries. *Energy Storage Mater.* **2022**, *51*, 733−755.
(137) Zhang, N.; Wang, J. C.; Guo, Y. F.; Wang, P. F.; Zhu, Y. R.; Yi, T. F. Insights on rational design and energy storage mechanism of Mn-based cathode materials towards high performance aqueous zinc-ion batteries. *Coord. Chem. Rev.* **2023**, *479*, 215009.
(138) Xu, Y.; Zhang, G.; Liu, J.; Zhang, J.; Wang, X.; Pu, X.; Wang, J.; Yan, C.; Cao, Y.; Yang, H.; Li, W.; Li, X. Recent Advances on Challenges and Strategies of Manganese Dioxide Cathodes for Aqueous Zinc-Ion Batteries. *Energy & Environmental Materials* **2023**, *6* (6), e12575.
(139) Zhang, N.; Cheng, F.; Liu, Y.; Zhao, Q.; Lei, K.; Chen, C.; Liu, X.; Chen, J. Cation-Deficient Spinel $ZnMn_2O_4$ Cathode in Zn(CF(3)SO(3))(2) Electrolyte for Rechargeable Aqueous Zn-Ion Battery. *J. Am. Chem. Soc.* **2016**, *138* (39), 12894−12901.
(140) Chen, H.; Cai, S.; Wu, Y.; Wang, W.; Xu, M.; Bao, S. J. Successive electrochemical conversion reaction to understand the performance of aqueous Zn/MnO_2 batteries with Mn^{2+} additive. *Mater. Today Energy* **2021**, *20*, 100646.
(141) Qin, Z.; Song, Y.; Yang, D.; Zhang, M. Y.; Shi, H. Y.; Li, C.; Sun, X.; Liu, X. X. Enabling Reversible MnO_2/Mn^{2+} Transformation by Al^{3+} Addition for Aqueous Zn-MnO_2 Hybrid Batteries. *ACS Appl. Mater. Interfaces* **2022**, *14* (8), 10526−10534.

https://doi.org/10.1021/cbe.3c00120
Chem Bio Eng. 2024, 1, 113−132